Mechanisms of cytotoxic brain edema

PhD thesis

Dr. Zsolt Zádor

Department of Neurosurgery
University of Szeged
Faculty of Medicine

2009.
Szeged

Original publications providing the base of to the thesis:

I. **Zador Z**, Magzoub M, Jin S, Manley GT, Papadopoulos MC, Verkman AS. 2008. Microfiberoptic fluorescence photobleaching reveals size-dependent macromolecule diffusion in extracellular space deep in brain. FASEB J. 22:870-9.

II. Uchida K *, **Zador Z***, Wang V, Mihaly A, Manley GT. 2009. Aquporin-4 deletion improves outcome by delaying the progression of cerebral edema following cortical impact. *Submitted for publication J Cereb Blood Flow Metab.*

III. Sorani MD*, **Zador Z***, Hurowitz E, Yan D, Giacomini KM, Manley GT. 2008. Novel variants in human Aquaporin-4 reduce cellular water permeability. *Hum Mol Genet.* 17:2379-89.

IV. **Zádor Z,** Weiczner R, Mihály A. 2008. Long-lasting dephosphorylation of connexin 43 in acute seizures is regulated by NMDA receptors in the rat cerebral cortex. Molecular Medicine Reports, 1:721-727.

*Authors contributed equally

Other original publications related to the thesis:

I. Fazekas I, Szakács R, Mihály A, **Zádor Z**, Krisztin-Péva B, Juhász A, Janka Z. 2006. Alterations of seizure-induced c-fos immunolabelling and gene expression in the rat cerebral cortex following dexamethasone treatment. Acta Histochem. 108:463-73.

II. Yang B, **Zador Z**, Verkman AS. 2008. Glial cell aquaporin-4 overexpression in transgenic mice accelerates cytotoxic brain swelling. J Biol Chem. 283:15280-6.

III. Jin S, **Zador Z**, Verkman AS. 2008. Random-walk model of diffusion in three dimensions in brain extracellular space: comparison with microfiberoptic photobleaching measurements. Biophys J. 95:1785-94.

Book chapters related to the thesis:

I. **Zador Z**, Bloch O, Yao X, Manley GT. 2007. Aquaporins: role in cerebral edema and brain water balance. Prog Brain Res. 161:185-94.

II. **Zador Z**, Stiver S, Wang V, Manley GT. 2009. Role of aquaporin-4 in cerebral edema and stroke. Handb Exp Pharmacol. 190:159-70.

III. **Zador Z**, Manley GT. 2008. Role of Aquaporins in Non-synaptic Mechanisms of Epilepsy. In Phil Schwartzkroin (Ed.), Encyclopedia of Epilepsy (*in press*). Berlin, Germany. Springer.

Conference abstracts related to the thesis:

I. Mihály A, Weiczner W, Krisztin-Péva B, Dobó E, Szakács R, Czigner A, **Zádor Z,** Batoka L, Tóth G. Seizure-dependent expression of *c-fos* in the neurons of the hippocampus *(IBRO International Workshop on Signalling Mechanisms in the Central and Peripheral Nervous System, Debrecen, January 2002)*

II. **Zádor Z.:** Decrease in connexin 43 phosphorylation rate in rat model of epilepsy. *(Scientific Students` Conference, University of Szeged, February 2005, 2nd Prize, Scientific Students` National Conference, University of Szeged, March 2005, 46th Congress of Medicine and Stomatology, Kotor, Montenegro, May 2005)*

III. **Zádor Z**, Mazin Magzoub, Songwan Jin, Geoffrey T. Manley, Marios C. P apadopoulos and A.S. Verkman Microfiberoptic fluorescence photobleaching reveals enhanced macromolecule diffusion in brain extracellular space of AQP4 knockout mice. 5th International Conference of Aquaporin 2007 Nara, Japan

List of abbreviations:

4-AP: 4-Aminopyridine

AQP4: aquaporin 4

CBF: cerebral blood flow

CBV: cerebral blood volume

CCI: controlled cortical impact

CHO: Chinese hamster ovary

CNS: central nervous system

CPP: cerebral perfusion pressure

CSD: cortical spreading depression

Cx43: connexin 43

ddAVP: Desmopressin

ECS: extracellular space

FITC: Fluorescent isothiocyanate

GAPDH: Glyceraldehyde 3-phosphate dehydrogenase

GJ: gap junction

HIV: human immunodeficiency virus

ICP: intracranial pressure

IOI: integrated optic imaging

MAP: mean arterial pressure

MCA: middle cerebral artery

NKCC1: Na^+-K^+-$2Cl^-$ Cotransporter 1

NMDA: N-methyl-D-aspartate

ns SNP: non-synonymous single nucleotide polymorphism

SNP: single nucleotide polymorphism

TMA: tetra methyl ammonium

Table of Contents

List of Figures

I. Introduction

I.1 Overview of edema mechanisms

Cerebral edema is characterized by the pathologic increase of brain water content paralleled by the expansion of cerebral tissue, which may appear as a common consequence of a number of diverse pathologies such as brain trauma, ischemia, hypoxia, hyponatraemia, tumors, inflammation, prolonged neuronal excitation (cortical spreading depression and seizures) and metabolic disturbances. Mechanistically, cerebral edema may either involve the cytotoxic swelling of brain cells, mainly astrocytes (cytotoxic edema) or the accumulation of fluid in the extracellar compartment (vasogenic or extracellular edema) (Klatzo 1967). In either setting one major consequence of brain swelling is the elevation of intracranial pressure as the rigid skull limits the brain expansion. Elevated ICP opposes cerebral perfusion pressure (CPP) thus reducing cerebral blood flow (CBF) leading to metabolic compromise (Oyesiku et al, 1990). Cerebral edema is also associated with the loss of autoregulation in the brain vasculature (Hemphill et al, 2001), which leaves the brain exposed to fluctuations in blood pressure and may lead to elevations in cerebral blood volume contributing to the expansion of the brain. Two relevant systemic pathologies related to brain trauma are cerebral salt wasting (Lu et al, 2008), and diabetes insipidus (Behan et al, 2008), both of which result in the disruption of plasma osmolarity (hypo- and hypertonicity respectively) which translates to alterations in brain water content. To battle all these consequences in the clinical arena, *multi-organ management* (pulmonary, circulatory and renal) is required to restore and maintain cerebral oxygenation, perfusion as well as maintain serum osmolarity. Our therapeutic tools however, *have remained unchanged for the past decades* while the control over cytotoxic cerebral brain swelling is still often insufficient. Therefore there remains a strong drive to uncover new avenues for the management of cerebral edema via exploring its mechanisms.

On the microscopic level, the development of cytotoxic edema is related to the excessive swelling of astrocytes. Under physiological conditions, these cells constitute a neurophil-spanning network, which maintains CNS environment. These cells have the ability to swell several times their size in cytotoxic edema, which result in the *contraction of brain extracellular space* (related to the expansion of astrocyte volume at the expense of ECS) and *collapse of capillary microvessels* embraced by the swollen astrocyte end-feet. Although these phenomenons have long been described (Van Harreveld and Khattab, 1967; Van Harreveld and Malhotra, 1967;

Vaz et al, 1997), we know little about their *in vivo* mechanisms, they never were translated into our bedside practice and thus received almost no clinical attention. We do know however, that the molecules facilitating the rapid trafficking of water trafficking inside the astrocyte network are the transmembrane water channel aquarporin 4 (AQP4) and the glial gap junction protein connexin 43 (Cx43). We hypothesized, that based on its role in facilitating astrocyte swelling, the function of AQP4 also promotes ECS contraction and microcapillary compression in cytotoxic edema. We also examined whether frequent mutations in the AQP4 gene -detected in a population of volunteers (Sorani et al, 2008)- would translate into altered channel function. Finally to further explore the development of cytotoxic edema on the level of the astrocyte network, we examined the regulatory changes of Cx43 in a seizure model.

I.2 Definition of cerebral edema

Cerebral edema is characterized by the pathological swelling of brain tissue due to a progressive increase in brain water content (Fishman et al, 1975). It is a frequent and feared clinical complication that develops in a broad range of cerebral insults such as ischemia (Badaut et al, 2002), trauma (Zador et al, 2007), tumors (Saadoun et al, 2002), hypoxia (Hackett et al, 2001), cardiac arrest (Hypothermia after Cardiac Arrest Study Group 2002), hyponatraemia (Adrogué et al, 2000) and metabolic disturbances (Rao et al, 2007). Clinically, the swelling of brain tissue translates to elevated intracranial pressure, which opposes cerebral perfusion pressure and in turn impair cerebral perfusion and metabolism (Figure 1). Klatzo categorized the mechanisms of brain swelling as cytotoxic edema and vasogenic edema (Klatzo 1967). The fundamental difference between the two edema types is that vasogenic edema appears in association with the compromise of blood brain barrier whereas the origin of cytotoxic edema is the rapid metabolic disturbance and/or osmotic swelling of CNS

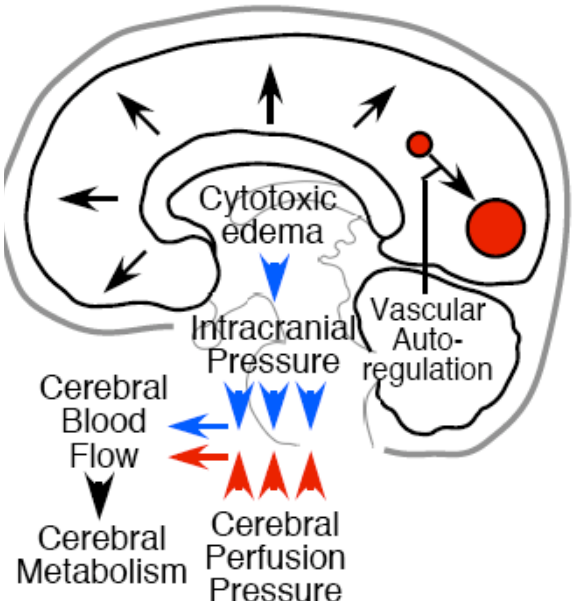

Figure 1. Impact of cerebral edema on brain physiology. The expansion of brain tissue translates into elevated intracranial pressure, reduced cerebral blood flow and impaired metabolism. There is also disruption in the vascular autoregulation resulting in hyperaemia.

cells (Figure 2). Although these two mechanisms coexist in most brain pathologies, there is typically an appreciable dominance of one type over the other in each disease. For example, vasogenic edema seems to dominate in tumors and cerebral abscesses, whereas cytotoxic edema develops in early phase of ischemic stroke, brain trauma and in the experimental model of water intoxication.

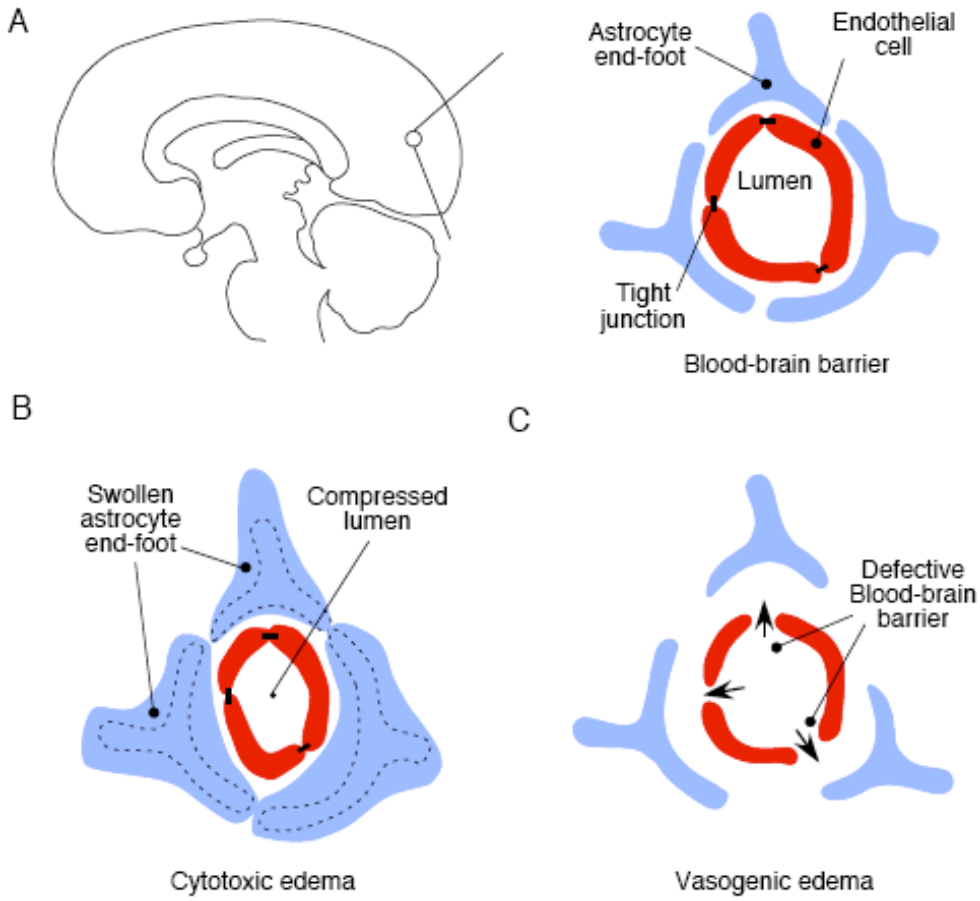

Figure 2. Klatzo's principals on the cellular mechanisms of brain swelling: cytotoxic and vasogenic (extracellular) edema. One major difference between these two processes is the intergrity of the blood brain barrier (A). In cytotoxic brain swelling (B), water accumulates in the perivascular astrocitic processes, while the blood brain barrier remains intact. During vasogenic edema (C), fluid accumulates in the extracellular space as it extravasates through the compromised blood brain barrier. Astrocyte end feet do not swell in vasogenic edema.

I.3 Clinical perspective of cytotoxic edema: From cellular mechanisms to the bedside

I.3.1 Cerebral physiology is supported by multi-organ systems

For the brain to maintain its functions it relies on proper supply of oxygen and nutrients together with clearance of metabolites via its circulation. At the same time it needs a stable osmotic and pressure environment secured by the blood and

cerebrospinal fluid composition together with a balance in production and circulation of the latter. Therefore from a whole body perspective, the following organ systems are involved in the maintenance of cerebral physiology: 1) *respiratory system* for adequate blood oxygenation and CO_2 ventilation 2) *the circulatory system* providing sufficient mean arterial pressure for cerebral perfusion 3) intact *production and circulation of cerebrospinal fluid* 4) the *urinary system* for maintaining circulating volume and blood osmotic status.

Cytotoxic edema is a multi-organ disease

In accordance cytotoxic cerebral edema can result from the disruption in any of the above mechanisms as seen in 1) hypoxia (high altitude disease), CO_2 intoxication *(respiratory system*) 2) Ischemic stroke, cardiac arrest (*circulatory system*) 3) Hyponatraemia in SIADH, Cerebral Salt wasting, Psychogenic polydipsia *(renal/urinary system)* 4) Drug intoxications (dinitrophenol, triethyltin, hexachlorophene, isoniazid) 5) Metabolic disturbances as seen in hepatic encephalopathy or Reye`s syndrome.

Cerebral edema is partly managed as a multi-organ disease (Figure 3).

Recommendations for management of cerebral edema include (Brain Trauma Foundation Guidelines 2007): monitoring and avoiding 1) hypoxia (saturation <90 Hgmm or PaO_2<60Hgmm) via proper ventilation and maintaining pulmonary functions 2) hypotension (SBP<90 Hgmm) via pressors and/or fluid resuscitation 3) avoiding prolonged elevation of intracranial pressure (keep ICP<20Hgmm) using a) hyperosmotic agents (mannitol, hypertonic saline) b) CSF drainage (extraventricular drain) c) hyperventilation (to decrease CBV) d) decompressive craniotomy (4) controlling hyponatraemia (serum Na<135mM). (Greenberg 2006)

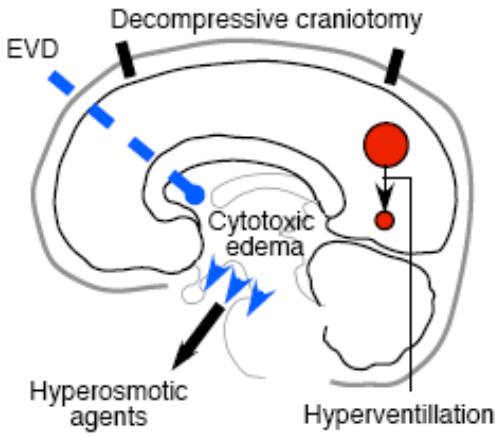

Figure 3. Current options in cerebral edema management. See text for details.

Multi-organ mechanisms of edema converged on the cellular level

The clinical aspects above may be translated to the level of the cellular mechanisms with the following. The swelling of CNS cells and subsequent expansion of the brain

develops in response to 1) disruption cell energy status/metabolism a consequent disruption of sodium and potassium pump in ischemia, hypoxia, cardiac arrest (see mechanism details in the following section) 2) osmotic swelling of cells in hyponatraemia 3) toxins disrupting cell metabolism (excessive neurotransmitter release, drug intoxication, hepatic encephalopathy). To give a detailed picture on the cellular mechanism of cytotoxic edema, the following sections will be focused on the main molecular candidates involved in cytotoxic astrocyte swelling.

I.4 Cellular mechanisms of cytotoxic edema in experimental water intoxication, traumatic brain injury and seizures

I.4.1 The swelling of astrocytes dominates cerebral edema in water intoxication, brain trauma and seizures.

Astrocytes contribute a significant portion of brain cells outnumbering neurons by a factor of 1.849-2.026 (depending on the cortical area) (Diamond et al, 1985; Terry et al, 1987). These cells carry a number of transporters that modulate ion, molecular (messengers, amino acids) as well as water movement across the cell membrane. Astrocytes also interact through gap junctions (GJ) to constitute a highly organized system: a neurophil-spanning cellular network that essentially acts as the nursing unit in maintaining CNS micro-homeostasis. Its specific functions include the buffering of ions, water, neurotransmitters and other metabolites that accumulate during physiological functions (neuronal firing) as well as in pathological states (seizures, ischemia, trauma) of the CNS (Bourke et al, 1980). In response to various noxas (potassium, glutamate, hypoxia, oxygen or nutrient deprivation) they have the capacity to swell several times their size (Solenov et al, 2004; Fabene et al, 2006). This volume increase contributes to the expansion of brain tissue, which translates to the macroscopic level as brain swelling. The direct relevance of astrocyte swelling in brain tissue expansion and its functional consequences were first shown by Manley et al when the impairment of cytotoxic swelling of astrocytes in vivo resulted in improved neurological outcome and survival after water intoxication and ischemia (Manley et al, 2000). These results imply, that astrocyte swelling is a key mechanism of cytotoxic edema and therefore is one of the targets for therapeutic control over brain swelling.

The experimental model of water intoxication is well established and has been broadly used as a prototype of pure cytotoxic brain edema (Manley et al, 2000; Trachtman et

al, 1992). The intraperitoneal administration of water together with desmopressin (ddAVP) results in serum hyponatraemia, which in turn reduces serum osmolarity. This creates an osmotic drive for water to enter the cells and thus produces cerebral edema.

Glial swelling following head trauma is seen to progressively increase in the first 24 hours following injury (Barzo et al 1997) as demonstrated by 1) slowed diffusion on diffusion weighted MRI imaging, 2) ultrastructural studies at the same time point have demonstrated cytotoxic swelling of pericapillary astrocytes together with the collapse of capillary lumen (Vaz et al, 1997).

During seizures astrocyte swelling is proposed to occur in response to the excess release of potassium and glutamate as well as other ions. Evidencing this notion are that 1) microdialysis studies in brain tissue during seizures revealed excess release of glutamate (Kovacs et al, 2003), potassium (Binder et al, 2004). 2) When reconstituting these circumstances in cultures, a marked swelling of astrocytes was seen. 3) Subsequent electron microscopy studies demonstrated a significant astrocyte swelling *in vivo* at 24 hours following seizure induction (Fabene et al, 2006). 4) Imaging studies showed decreased DWI signal in parallel with the astrocytic swelling further supporting the development of cytotoxic edema following acute seizures (Fabene et al, 2006).

I.4.2 Disrupted osmotic balance causes astrocyte swelling.

One of the generally proposed mechanisms for astrocyte swelling in pathological states -including models of head injury- are the activation of Cl-/HCO- and H+/Na+ exchange secondary to the excess hydration of intracellular CO2. The functional significance of these transporters was demonstrated by the ability of Cl-/HCO3- blockers (indanyl and fluorenyl compounds) to reduce astrocyte swelling in vitro and in vivo (Kimelberg et al, 1990). Another set of studies show a dynamic rise of intracellular Na+ and Ca++ paralleled by a drop in K+ in response to energy deprivation (hypoxia, hypoglycemia). The intracellular levels of ATP -used as a measure of energy depletion- showed positive correlation with the magnitude and velocity of alterations in ion levels (Silver et al, 1997).

In response to astrocyte swelling regulatory processes of the cell are initiated to reconstitute its volume. These mechanisms include the function of volume activated anion channels, the release Glutamate, Taurine and D-Aspartate to reduce

intracellular osmolarity (Kimelberg et al, 1995), as well as the inhibition of glutamate and aspartate uptake. The volume regulatory mechanisms for swelling induced by elevated K are proposed to be linked to the NKCC1 cotransporter in astrocytes (Su et al, 2002).

These mechanisms of highly organized transmembrane ion transport create and osmotic drive for water to pass through the cell membrane as well as via the astrocyte network. Therefore the next key players to be discussed in astrocyte swelling are the channels granting intercellular and transmembrane water flux.

I.5 Molecules facilitating water trafficking and volume changes in astrocytes: water channels and gap junction proteins.

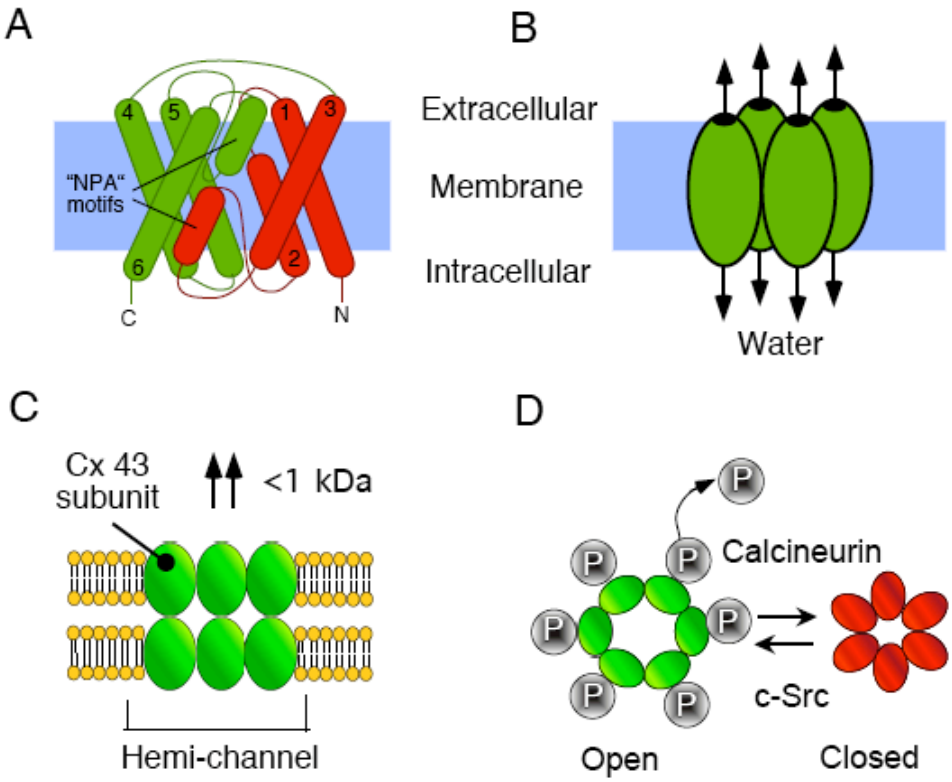

Figure 4: Channel structure and function of aquaporins (A and B) and gap junction protein connexin 43 (C and D). Aquaporins are constituted of 6 transmembrane helices (A) and permit selective water flux driven by the osmotic gradient (B). Gap junction protein connexin 43 consists of two adjacent hexameric protein monomers allowing trafficking of molecules smaller the 1kDa (C). Channel permeability is regulated by the phosphorylation status of the connexin 43 subunits determined by the kinase (c-Src)-phosphatase (Calcineurin) equilibrium.

I.5 .1 Aquaporin 4: the glial water channel in the brain

The selective water flow through AQPs is passive, driven by osmotic gradients (Verkman et al, 2005; 2006). To date, over 12 different members of the AQP family have been identified, and a number of them have been shown to contribute to rapid

water flux in various tissues including the kidney, lung, gastrointestinal tract, and in the CNS (Agre et al, 2002; Verkman et al, 2005; 2006). The glial water channel aquaporin-4 (AQP4) was first cloned from rat lung and was subsequently found to be expressed in various fluid-tissue interfaces in the brain, such as astrocytic processes adjacent to cerebral capillaries, pial membranes lining the subarachnoid space and ependymal cells of the brain ventricles (Figure 5). The strategic localization at these tissue-water interfaces, and the high water permeability, makes AQP4 an important route for transporting water into- and out of the brain parenchyma. A large body of evidence from transgenic mice deficient in AQP4 demonstrated the role of this water channel in cytotoxic and vasogenic edema (Verkman et al, 2006). During cytotoxic edema, when water moves into the cellular compartment, AQP4 was found to facilitate cellular swelling (Manley et al, 2000). In vasogenic edema, when edematous fluid accumulates in the extracellular space, the clearance of edema fluid is facilitated by AQP4 (Papadopoulos et al, 2004). These key functions of AQP4 in cerebral water balance suggest this channel as potential therapeutic target in the treatment of cerebral edema.

I.5.2 Variants and altered expression of the AQP4 gene

A number of studies have shown changes in AQP4 expression in focal brain injury

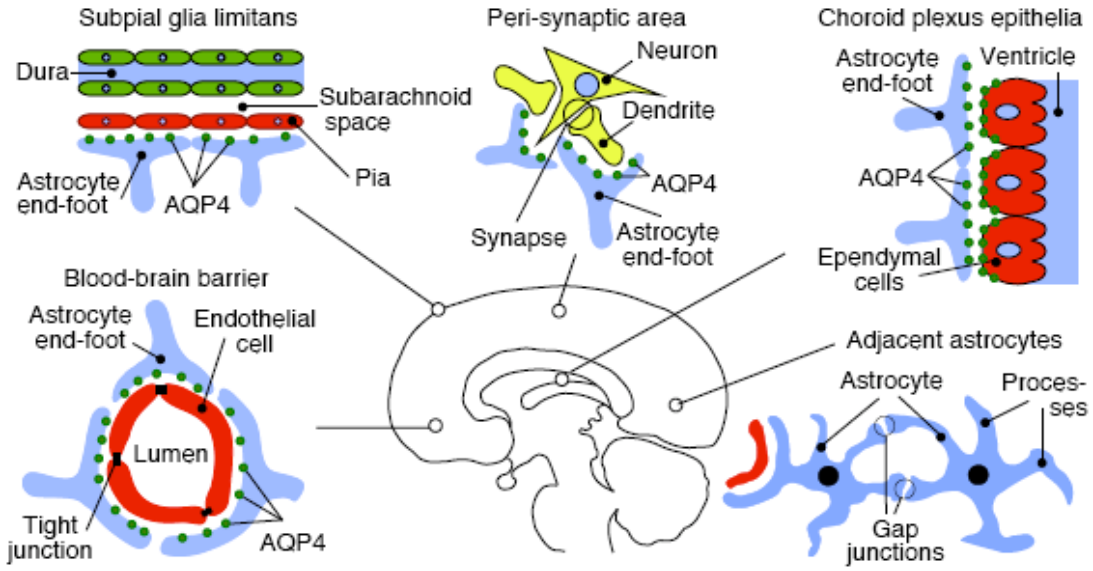

Figure 5: Localization of the glial water channels and the gap junction proteins at strategic water trafficking sites in the brain. AQP4 is polarized at water brain interfaces such as the perivascular processes of astrocytes, the glial limitans facing the pial membrane, perisynaptic sites, ependymocytes and astrocytes bordering the ventricles. The gap junction protein connexin 43 is exclusive to astrocytes and provides low rsistance intercellular coupling.

(Neal et al, 2007), brain abscess (Bloch et al, 2005), meningitis (Papadopoulos et al, 2005), tumors (Saadoun et al, 2002) in epilepsy (Lee et al, 2004) and also in astrocytes cultures subjected to hypoxia (Fu et al, 2007). Levels are also altered in Duchene's muscular dystrophy (Wakayama et al, 2002), HIV dementia (St. Hillaire et al, 2005), lupus (Alexander et al, 2003), neuromyelitis optica, multiple sclerosis (Sinclair et al, 2007), Crohn's disease and infectious colitis (Hardin et al, 2004). Changes in AQP4 expression translate into altered water permeability of the cellular membrane, which impact their ability to swell.

A number of variations in the 4th exon of AQP4 were examined for a potential role in traumatic brain edema with negative results (Romeiro et al, 2007). Further studies however, found that patients with one of the AQP4 variant (rs9951307) developed worse cytotoxic edema in malignant MCA strokes (Kleffner et al, 2008). This implies that specific AQP4 polymorphisms may alter water permeability in a way to facilitate cytotoxic brain swelling.

I.5 .3 Gap junction protein, connexin 43 in the brain

Gap junctions (GJ) are multi subunit channels that provide low resistance communication between adjacent cells in various tissues including the brain (Nagy and Rash 2000), heart (Duff et al, 2006), skin (Qui et al, 2003) and testis (Sridharan et al, 2007). The GJs provide neuronal and glial coupling for ion and water, and are also considered as candidates in the pathogenesis of epilepsy (Nemani et al, 2005) as well as the regulation of brain water homeostasis. GJs are composed of connexin protein subunits, which form two hexameric connexon channels on the adjacent cell surfaces (Musil et al, 1991; Martin et al, 2004) (Figure 4C and 5). Connexins are encoded by a large multigene family, with more than 20 members in mammals (Willecke et al, 2002). Certain members of the connexin family are cell-specific in their expression: connexin 36 is detected in neurons (Rash et al, 1998), whilst connexin 43 is present in astrocytes and ependymal cells of the CNS (Condorelli et al, 2003). The connexon is assembled in the endoplasmic reticulum and the Golgi-apparatus, and inserted into the cell membrane to form an „unopposed" connexon hemichannel (De Sousa et al, 1993, Martin et al, 2004), which subsequently forms an intercellular GJ with the similar hemichannel of an adjacent cell (Martin et al, 2004). The conduction properties of the gap junction formed by connexin 43 are influenced by the phosphorylation rate of the connexin protein subunits: dephosphorylation causes the opening of the channel (Sáez et al, 2003) (Figure 3D), decreases the formation of GJs (Sáez et al, 2003, Toyofuku

et al, 2001), and results in the closure of GJs. GJs allow the passive flow of molecules below 1kDa (Simpson et al, 1977), therefore the regulation of connexons plays an important role in water-ion homeostasis and volume transmission of the brain, in both physiological and pathological conditions (Simard and Nedergaard, 2004).

I.5.4 Astrocytic gap junction function is altered in CNS pathologies

Astrocyte cultures and brain slices exposed to seizure equivalent environments such as high $[K^+]_o$ and increased glutamate concentration, displayed delayed dephosphorylation of connexin 43, which translates into decreased coupling of astrocytes (Nagy et al, 2000). The reduction of intercellular coupling impairs efficient trafficking of ions and metabolites and as such it is likely to have an impact on glial cell volume in seizure. In another set of studies conditional knockout mice lacking connexin 43 displayed a slow decay of [Ko+] subsequent to stimulus train (Wallraff et al, 2006), indicating that astrocytic GJ facilitate intercellular K+ diffusion. A likely mechanism is that open GJ contribute to low-resistance intercellular coupling between neighboring cells (Flagg-Newton et al, 1979), allowing the passive movement of all particles under 1 kDa (Simpson et al, 1977.). Therefore, GJs facilitate the redistribution and buffering of several ions and molecules such as K+ (Wallraff et al, 2006; Walz et al, 1993) or glutamate (Goldberg et al, 2004), accumulated during generalized tonic-clonic seizures (GTCS). This phenomenon has been referred to as 'spatial buffering' (Simard and Nedergaard, 2004).

I.6 Cytotoxic cell swelling causes contraction of brain ECS and microcapillary compression. (figure 6)

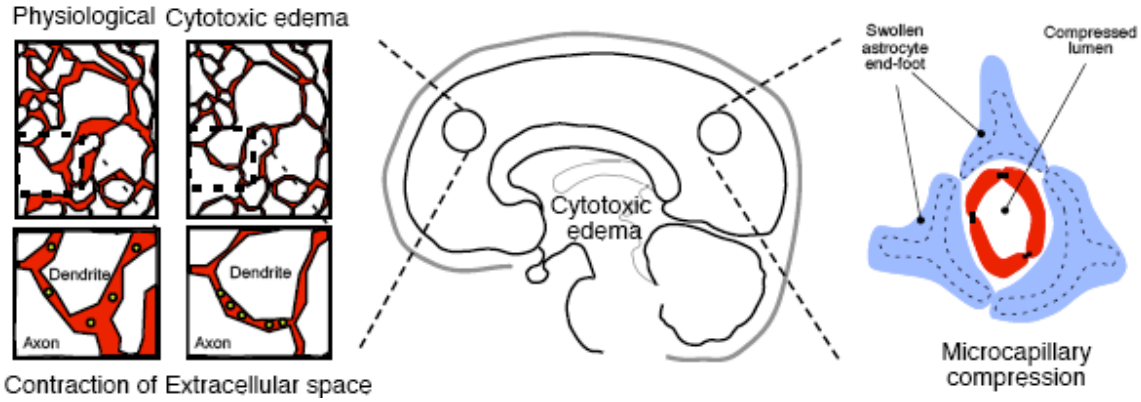

Figure 6. Ultrastructural consequences of cytotoxic edema: contraction of the extracellular space and the compression of microcapillaries. *Left:* During cytotoxic swelling, cells expand at the expense of the extracellular space resulting in the contraction of the ECS. *Right:* the rapid swelling of perivascular astrocitic foot processes results in the compression of capillary endothelia, compromising the vessel lumen.

In cytotoxic edema, astrocytes expand at the expense of brain ECS. This phenomenon was first described by van Harreveld in circulatory arrest (Harreveld and Malhotra, 1967) and cortical spreading depression (Van Harreveld and Khattab, 1967) by demonstrating 1) a significant increase in brain tissue resistance in relation to 2) narrowed intercellular distances on brain electronmicrographs. Subsequent measurements using real time iontophoresis have reinforced this observation in brain ischemia and cortical spreading depression. In physiological states brain ECS was measured to occupy ~20% of total brain volume but decreased to 7% and 5-9% in ischemia (Zoremba et al, 2008) and cortical spreading depression (Mazel et al, 2002) respectively. Subsequent studies using cortical surface photobleaching has demonstrated the significant (>10 fold) slowing of macromolecular diffusion following seizures or cytotoxic edema. (Binder et al, 2004).

A series of studies showed that perivascular astrocyte swelling was accompanied by the narrowing of capillary lumen (Figure 6). Transmission electronmicroscopy showed decreased luminary diameter in brain capillaries accompanied by astrocyte swelling. In accordance 3D corrosion casts of brain tissue from head injured patient supported this notion as the characteristic angioarchitectonic changes of longitudinal folds, sunken surfaces with craters, and a significant flattening with reduction of lumen was seen (Wasterlain et al, 1968, Rodríguez-Baeza et al, 2003). As a follow up on the consequences of these morphological changes, Meinig at al have observed a CBF reduction independent of the opposing effect of ICP on CPP following a graded series of water intoxication experiments. This suggested that the microcapillary collapse seen on the ultrastructural level translates to the impairment in cerebral blood flow. (Meinig et al, 1973).

I.7 Aims

In the current thesis we aim to dissect the mechanism behind the ECS contraction and microcapillary compression in cerebral edema in relation to AQP4 and connexin 43 function (Figure 6). We hypothesized; that the glial water channel AQP4 facilitates these two processes since it also promotes astrocyte swelling. To further elucidate the mechanisms of cell swelling responsible for the development of cytotoxic edema, we tested the functional relevance of AQP4 variants using a cell culture model. Finally we also examined the regulatory changes in gap junction proteins in relation to cytotoxic swelling in a seizure model.

II. Materials and Methods

Animals

We used male, weight-matched (25–30 g) wild-type and AQP4 null mice (Ma et al, 1997) in a CD1 genetic background. Protocols were approved by the University of California, San Francisco Committee on Animal Research.

In other sets of experiments male Wistar rats weighing 200-250 g were bred in the Central Animal House of the University of Szeged under standard conditions with *ad libitum* access to food and water. All experiments were conducted in accordance with the European Community Council Directive of November 24, 1986 (86/609/EEC) and the Hungarian Animal Act (1998).

Construction of dual-lumen microfiberoptic

Single, multimode optical fibers, consisting of a 62.5-μm diameter core, were purchased from ThorLaboratories (Newton, NJ, USA). After the distal 4 cm of their cladding was stripped, each fiber was chemically etched by immersion of the fiber tip for 10 min at the interface of 48% aqueous hydrofluoric acid and xylene (Sigma-Aldrich Corp., St. Louis, MO, USA). The fiber tip was then rinsed with distilled water and dried, and the process was repeated several times to create a tapered fiber shaft with a 2- to 5-μm diameter tip, as visualized using a Leica DM 4000B microscope. A very thin coating (~10 nm) of aluminum was deposited by rotary sputtering (Evaporated Coatings Inc., Willow Grove, PA, USA) over a length of ~7 mm from the tip, excluding the tip itself.

To achieve efficient and standardized dye delivery in deep brain structures, a double-lumen micropipette was fabricated using borosilicate glass microcapillaries. For dye introduction, a single-barrel microcapillary without filament (inner diameter/outer diameter 0.75 mm/1 mm; FHC Inc., Bowdoin, ME, USA) was pulled on a vertical pipette puller (David Kopf Instruments Inc., Tujunga, CA, USA) to a 5-μm diameter tip and a bend of 60° was created 5 mm from the tip (Figure 7A). A second pulled microcapillary was created as a guide for the optical fiber. The guide consisted of a 3-mm-long glass microcapillary with tip diameter 100 μm to allow the microfiber to pass freely through the lumen. The dye-introducing and fiber-guide microcapillaries were immobilized with glue on a small glass platform, with the tip of the guide microcapillary positioned 2–2.5 mm proximal to the tip

Instrumentation for microfiberoptic photobleaching

Bleaching was done using an epifluorescence apparatus as described previously (Seksek 1997), with modifications. The first-order beam of an argon ion laser (1 W at 488 nm) was diffracted by an acousto-optic modulator and focused using an 20x objective lens (numerical aperture, 0.25; Zeiss air) onto the back of the optical fiber that contained an FC-type connector (Figure 7*B*). Bleaching was accomplished by increasing laser illumination intensity 3000- to 6000-fold for 0.1–20 ms to reduce fluorescence by 30–40%. The low intensity of the probe beam used for acquisition produced ~1% fluorophore bleaching for continuous recordings up to 5 s. Sample fluorescence collected by the optical fiber and objective lens was filtered (490 nm dichroic mirror, 510 nm long-pass filter), detected by a photomultiplier, amplified, and digitized at 14-bit resolution. Fluorescence was sampled continuously over 200 ms before the bleach pulse, at rates of up to 100 Hz for 5 s after bleaching, and at up to 4 Hz (shutter opened for 20 ms per acquisition) for longer times.

Microfiberoptic photobleaching measurements in mouse brain

Mice were anesthetized by i.p. injection of Avertin (2,2,2-tribromoethanol, 125 mg/kg) and immobilized in a mouse stereotactic frame (MyNeuroLab, St. Louis, MO, USA). Additional Avertin was administered as needed to maintain anesthesia. Core temperature was maintained at 37–38°C using a feedback-controlled rectal probe and heating pad. In some experiments water intoxication was produced by i.p. injection of water (10% body weight) together with 1-deamino-8-darginine vasopressin (0.4 μg/kg). The skull surface was exposed by a midline scalp incision, and the skin was retracted. In some experiments the temporal muscle was secured with suture to minimize motion artifact from muscle contraction. The intact cortical dura and underlying brain surface were exposed with great care by a craniectomy using a Foredom micromotor drill (MyNeuroLab) with a 1-mm diameter burr and microsurgical instrumentation. The site of the craniectomy was marked using stereotactic coordinates of the brain region to be studied, according to the Paxinos mouse brain map (Franklin 1997). The mouse brain in stereotactic coordinates consists of frontal cortex (bregma +1 mm) were centered 1.2–1.4 mm lateral to midline. In most experiments two overlapping 1-mm diameter burr holes were created to give an approximately rectangular 1.5- 1-mm space for insertion of the double-barrel microcapillary. In experiments involving topical dye application, a larger, 5-mm diameter craniectomy was made to expose a larger area of dura for dye

penetration. For photobleaching measurements, the tip of the dye introducing microcapillary of the dual-microcapillary device was inserted gradually into the brain to specified stereotactic coordinates under positive injection pressure to produce a fluid infusion rate of 0.15 μl/min. The site of insertion was specified with high precision using the micropositioning system of the stereotactic frame, taking into account the dimensions of the dual-lumen microcapillary. Artificial cerebrospinal fluid (aCSF) (145 mM NaCl, 4 mM KCl, 1 mM MgCl2, 2.5 mM CaCl2, 1 mM KH2PO4, and 10 mM glucose; pH 7.4) containing FITC-dextran (70 kDa; 50 mg/ml) was infused intraparenchymally at a rate of 0.15 μl/min for 15 min using a Hamilton syringe and infusion pump. Measurements were done 20 min or more after dye infusion to allow for fluorescent dye penetration into the brain tissue surrounding the injection site. The optical fiber was mounted on an independent, micron-resolution micromanipulator (World Precision Instruments Inc., Sarasota, FL, USA) for insertion to specified depths (accuracy 5 μm) through the guide microcapillary. After removal of the bone flap, the dura was irrigated continuously with aCSF warmed to 37°C, and body temperature was maintained at 37–38°C. In some control experiments, FITC-dextran was applied topically as described previously (Binder et al, 2004).

Diffusion measurements in solutions and gels

Microfiberoptic photobleaching measurements were made in solutions consisting of aCSF containing 70 kDa FITC-dextran. Measurements were also performed in aCSF-glycerol solutions (0–50% w/v glycerol) and in gelatin gels (2–60 mg/ml gelatin). The microfiber tip was inserted 400 μm into a 200 μl volume of solutions/gels in microcuvettes.

Analysis of microfiberoptic photobleaching data

Recovery curves generally contained a “fast” acquisition (500 data points over 5000 ms) followed by a “slow” acquisition (20–160 data points over 10–80 s, illumination shuttered between collections). At each location, three to nine photobleaching recovery measurements were made, with the fiber tip displaced 5–10 μm in depth to avoid repeat measurements at the exact same location. Each set of three to nine curves from one location was averaged for curve fitting. For most experiments fluorescence recovery data, $F(t)$, were fitted to the equation (Axelrod et al, 1976): $F(t) = (F_0 + [R(F - F_0) + F_0](t/t_{1/2}))[1 + (1/t_{1/2})]^{-1}$, where F is the prebleach fluorescence, F_0 is the fluorescence immediately after bleaching, R is the mobile fraction (percentage recovery), and $t_{1/2}$ is the half-time for recovery. This equation was found empirically

to provide a very close fit to the data for determination of $t_{1/2}$ as the single parameter describing the kinetics of fluorescence recovery. The relative diffusion coefficient in aCSF *vs.* brain (Do/D) was computed from $t_{1/2}$ measured in brain *vs.* aCSF: $D_o/D = t_{1/2\ brain}/t_{1/2\ aCSF}$. Determination of D_o/D is thus comparative and model/geometry-independent.

Controlled cortical impact injury model

Male mice were anesthetized with 2,2,2,-tribromoethanol (150 mg/kg, intraperitoneal, Sigma-Aldrich, St.Louis, MO). The head was immobilized and the skull was exposed by a midline incision (Figure 11A). A craniotomy of 5 mm diameter was done on the parietal bone to expose the intended site of impact. The bone flap was removed without damage to the dura (Figure 11B). The 3 mm diameter tip of impactor was positioned adjacent to the dural surface under the guidance of a surgical microscope. The velocity of impact was set at 4.5 m/s, with an impact depth of 1.7 mm and dwell time of 150 ms. Immediately after injury, the bone flap was repositioned and fixed with tissue glue (Abbott Laboratories, North Chicago, IL) followed by closure of the skin with sutures.

Electron microscopy.

The animals were deeply anesthetized with diethyl-ether and perfused transcardially with 250 ml of 0.1 M PBS pH 7.4 followed by 300 ml of fixative (1% paraformaldehyde and 1% glutaraldehyde in phosphatebuffered solution, pH 7.4). Samples of the right parietal cortex were prepared for electron microscopy. Following thorough rinsing, the tissue blocks were incubated in an aqueous solution of 1% OsO4 and 5% K2Cr4O7 (1:1). The samples were dehydrated then incubated in 1% uranyl-acetate and embedded in Durcupan epoxy resin (Fluka, Buchs, Switzerland). Semithin sections were cut on an ultramicrotome (Ultracut E, Reichert-Jung, Vienna, Austria) and stained on object glasses with a 1:1 mixture of 1% methylene blue and 1% azure II blue. The samples were then coverslipped with DPX mountant and analysed under a light microscope (Nikon E600, Nikon Co., Tokyo, Japan). Ultra-thin sections were cut of the same blocks and collected on 200-mesh copper grids. The preparations were then contrasted with 5% uranyl acetate and Reynolds lead citrate solution. Specimens were viewed under a Philips TM10 transmission electron microscope (Eindhoven, The Netherlands). Imaging was acquired with a computer-assisted digital camera (MegaView II, Soft Imaging Systems, Munster, Germany).

Approximately 900 μm2 of sample surface was viewed systematically through all

neocortical layers of the parietal cortex, and 12±2 capillary cross sections were examined in each specimen. The total area of the so-called neurovascular unit, which consists of the capillary lumen, the surrounding endothelium and the astrocytic end-feet covering the basal lamina of the microvascular endothelium, was measured (Image Pro Plus 4.5 morphometric software; Media Cybernetics, Silver Spring, MD, USA).

In vitro culture system for expressing AQP4 variants

We created stably transfected cells (CHO Flp-In system) expressing reference and variant AQP4 –extracted form a cohort of volunteers (Sorani et al, 2008) for use in a water permeability assay (Figure 13). (detailed procedure see Sorani et al, 2008).

Protein expression: Western blot, Cell surface biotinylation

For quantitating AQP4 expression in the entire cell, protein extraction from cell lysates was done as described previously (Yang et al, 1997) and Western blot was preformed as detailed in Binder et al, 2004. Cells were lysed using Cell surface biotinylation was used to quantify the functional pool of AQP4 protein trafficked into the cell membrane. Cell cultures were grown to confluency in T75 flasks and incubated in ice cold saline solution containing 0.5mg/ml Sulfo-NHS-Biotin (Pierce) at 4˚C for 30min. Cultures were washed 2 times in saline and excess biotin was quenched with 3% BSA followed by another set of rinsing. Cells were then removed from the flasks, lysed in buffer containing 0.1% SDS in PBS, 20µg/ml PMSF. The cell lysate was spun at 10,000g and the supernatant was collected. Following protein concentration measurement (BCATM Protein Assay Reagent, Pierce), a 5µg protein aliquot was kept for loading control, and 50µg of protein was incubated with a 100µl slurry of streptavidin beads (Pierce) overnight at 4C˚ to isolate the membrane proteins. Centrifuging at 10000g for 1min pulled down biotin-streptavidin complexes, and following extensive washes the bound protein was eluted in Lamely buffer at 37 ˚C.

Water permeability measurements

We assessed osmotic water permeability (P_f), in cells with the well-established method of stopped-flow light scattering (Verman 2000) using a Hi-Tech Sf-51 instrument (Figure 14). Cells suspensions were exposed to hypo or hyper-tonic solution, and cell swelling or shrinking was measured by a change in diffraction of

light. The water permeability kinetics of increasing cell volume was assessed from the time course of 90° scattered light intensity at 530 nm wavelength. Osmotic water permeability coefficients were calculated from the $t_{1/2}$ of the exponential curve fitted to the time course light scattering as previously described (Verman 2000, Yang et al, 1997). Relative P_f was deduced from the $t_{1/2}$ values normalized to AQP4 membrane protein expression. Three different passages of cells were used for relative water permeability measurements and at least five curves of each cell line were analyzed. Results are reported as mean + S.E.M., and significance was assessed by Student's t-test at a level of p=0.05.

Seizure induction in rats

Rats were injected intraperitoneally (i.p.) with 4-AP (Sigma, 5 mg/kg 4-AP dissolved in physiological saline, 1.0 mg/ml concentration). The control animals received the same volume of physiological saline i.p. Dizocilpine maleate (MK-801, Sigma) dissolved in physiological saline was administered i.p. 10 min before 4-AP administration at a dose of 1 mg/kg (Mihaly et al, 1990; Szakacs et al, 2003). Animal seizure behavior was evaluated as previously described by measuring the latency of symptoms (Mihaly et al, 1990). Animals were observed at 1, 3 and 24 h from the time of 4-AP injection, with 3 repeats in each group. The pharmacological effect of MK-801 was evaluated separately (10-10 animals in each group).

Protein measurements, dedicated preparation for connexin 43

Neocortex samples were obtained as described above and frozen in liquid nitrogen. Regarding the solubility of the different phosphorylated forms of connexin 43 (Musil et al, 1991), no detergents were used during protein purification. The second portion of the samples was homogenized in ice cold buffer (pH 7.2) containing 20 mM HEPES, 0.5 mM EDTA and the following protease inhibitors: 1 mM phenylmethylsulfonyl fluoride (PMSF), 1 μM pepstatin A and 2 μM leupeptin (Christ 2003). To preserve the phosphorylated forms, 10 mM of the phosphatase inhibitor Na3VO4 was added to the lysis buffer in specified samples. Homogenates were centrifuged at 20,000 g for 30 min at 4˚C, then the pellet was resuspended in homogenization buffer. Alkaline phosphatase treatment was carried out with some modifications (Wang et al, 1995.). With Na3VO4 excluded, 70 μg of pre-cleaned lysate was equilibrated against 100 mM Tris (pH 8.0), 100 mM NaCl, 5 mM $MgCl_2$, 2 mM PMSF and 0.6% SDS. Half the sample was treated with 2 U/sample alkaline

phosphatase at 37˚C for 4 h, and the other half was incubated untreated. The reaction was terminated by the addition of 200 mM Na3VO4. Samples were re-dissolved in 10% acrylamide gel with a prolonged run-time (~2.5 h at 200 V) to separate the different forms of connexin 43 (all chemicals used for protein blotting were purchased from Sigma). Protein was transferred by the semi-dry method (Bio-Rad) onto polyvinylidene difluoride membranes (Amersham) at 11 V for 50 min. Blots were blocked for 1 h at room temperature with 5% skimmed dry milk and probed with a 1:1,000 dilution of rabbit polyclonal connexin 43 antibody raised against the 252-271 fragment of the protein distant from the known sites of phosphorylation (Malfait et al, 2001) for 1 h at room temperature. The connexin 43 antibody was a generous gift from Professors Bernard Himpens and Johan Vereecke, Laboratory of Physiology, KU Leuven, Belgium. Following extensive washes in phosphate-buffered saline PBS (pH 7.4) containing 0.1% Tween, the blot was incubated with alkaline phosphatase tagged anti-rabbit secondary antibody (Amersham) at a dilution of 1:10,000 for 1 h at room temperature. ECF™ substrate (Amersham) was added and the blots were quantitated with ImageQuant (Typhoon™ 9400 Variable Mode Imager, Molecular Dynamics) as described above.

To detect AQP4 from cell lysates or cell surface biotinylation extracts Cells were homogenized in buffer containing 250mM sucrose in PBS and 20ug/ul PMSF. Homogenate was centrifuged at 15,000 g and after careful assessment of the protein-signal correlation, 6µg of supernatant was loaded onto 10-12% polyacrylamide gels (Invitrogen). Protein was transferred overnight at 15V at 4 °C onto PVDF membranes (Amersham). After 1h blocking with 3% skimmed milk (Bio-Rad), blots were probed with primary antibody against AQP4 (Chemicon) for 1h at a dilution of 1:1000 in 1% BSA. Following extensive washes in Tris-Buffered Saline Tween (TBST), blots were incubated with horseradish peroxidase conjugated secondary antibody (1:5000) and detected with Electrochemiluminescence (ECL) kit (Amersham). To confirm the specificity of membrane protein detection, blots were stripped according to the manufacturer's instructions and re-probed for the intracellular housekeeping protein glyceraldehyde-phosphate dehydrogenase (GAPDH) with a 1:2000 dilution of monoclonal antibody from Chemicon. This was followed by extensive washes and detection using antimouse peroxidase conjugated antibody. Densitometry of the protein bands were assessed with ImageJ, and AQP4 expression was normalized to GAPDH expression.

Statistical analysis.

Data are presented as the means ± STDEV. Statistical analysis of the data from the indicated groups were performed using the Student's t-test and the Newman-Keuls test or one-way analysis of variance (ANOVA) followed by the Bonferroni *post hoc* test.

Results

R.1 The effect of AQP4 deletion on ECS diffusion in cytotoxic edema.

Current methods for measuring ECS diffusion are either limited to the superficial layers of brain tissue (~200 μm), or suitable only to investigate the diffusion of small, biologically non-relevant molecules (TMA). To bypass these obstacles we have developed a novel system for diffusion detection in deep brain structures using a microfiber optic probe (Figure 7) and fluorescent recovery after photobleaching (FRAP) (Figure 8).

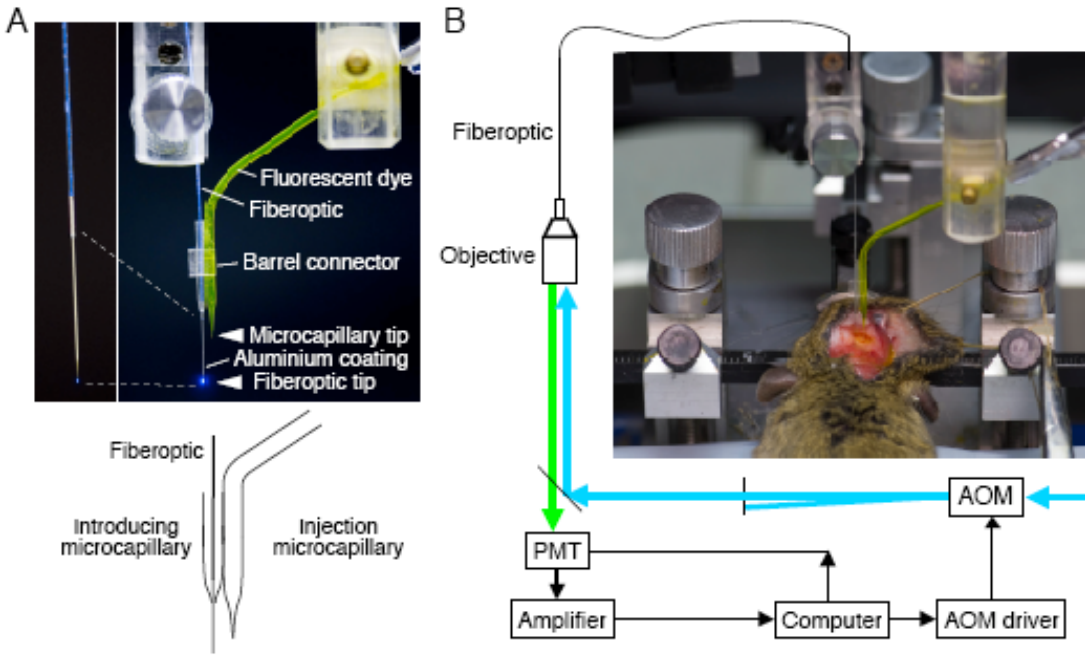

Figure 7: Microfiberoptic photobleaching apparatus for *in vivo* measurement of dye diffusion in the ECS in deep brain structures. *A*) Double-lumen microfiberoptic device, with dye-introducing and optical fiber-introducing microcapillaries. Photograph shown in the top panel, with inset (at the left) showing aluminized microfiberoptic tip. Schematic shown in the bottom panel. *B*) Schematic diagram of photobleaching apparatus showing laser illumination of the back end of a multimode microfiberoptic. AOM acousto-optic modulator; PMT photomultiplier. Photograph showing mouse head immobilized in a stereotactic frame with double-lumen device inserted through burr holes. See text for details.

The new microfiberoptic measurement system with double lumen microcapillary dye introduction was validated by diffusion measurements in artificial solutions and gels. Figure 9A *left* shows fluorescence recovery curves after microfiberoptic photobleaching of aqueous FITC-dextran (70 kDa) made viscous with different concentrations of glycerol. As expected, the fluorescence recovery was slowed with increasing solution viscosity. Recovery curves fitted closely to the semiempirical equation given in the Materials and Methods section with fitted parameter $t_{1/2}$, the apparent half-time for fluorescence recovery, which is inversely proportional to the diffusion coefficient. FITC-dextran diffusion was slowed 4.5-fold at 50% (vol) glycerol, in agreement with its relative solution viscosity of 4.6. Figure 9B *right*

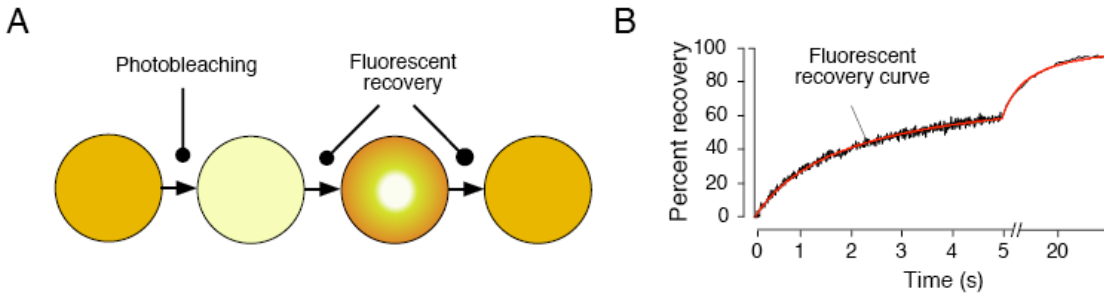

Figure 8: Principles of FRAP. A: The volume of tissue loaded with the phlorophore is bleached using a high intensity LASER beam. A subsequent recovery in fluorescent signal is seen due to the diffusion of fluorophore from the surrounding tissue into the illuminated volume. B: The dynamics of signal recovery is depicted by the signal intensity plotted as a function of time. The time constant of fitted curve is proportionate to the diffusion constant of the dye in the tissue.

shows fluorescence recovery with the microfiberoptic inserted into gelatin gels of increasing concentration to simulate brain tissue. FITC-dextran was introduced into the gels using the double-lumen device. The microfiberoptic was inserted at a depth of 400 μm in the gels, equivalent to central brain cortex. Recovery curves again fitted well to a single-component diffusion model with 100% fluorescence recovery, with reduced recovery rates ($t_{1/2}$) (Figure 9 A *right*, inset) with increasing gelatin concentration. FITC-dextran diffusion in saline *vs.* gels (*D*o/*D*) was 4 at a gelatin concentration of 20 mg/ml, similar to the slowing found in brain cortex (see under). In control studies, fluorescence recovery did not depend on the depth of insertion of the optical fiber (200–800 μm). Initial experiments were done in cerebral cortex using the double-lumen device (Figure 9B *left*). At an insertion depth of 400 μm, fluorescence recovery data fitted well to a single component diffusion model with *D*o/*D* 4.2 and 98% fluorescence recovery (Figure 9B *left*). The 4-fold slowing of FITC-dextran diffusion in brain cortex is comparable to our previous data of 3-fold slowing obtained by cortical surface photobleaching (Binder et al, 2004). The lower fold slowing as measured by surface photobleaching may be related to the relatively higher abundance of white matter tracts in the superficial layers of the cortex. In a control study to exclude the effects of fluid infusion from the double-lumen device, diffusion was compared after loading brain ECS with FITC-dextran using the infusion method *vs.* topical dye application and diffusion across the intact dura. *D*o/*D* measured at a depth of 400 μm did not differ significantly with the two loading methods (Figure 9B *right*). Figure 10 A shows the area of fluorescent dye staining after loading by infusion and a 15-min incubation. As seen by fluorescence imaging of freshly cut brain, the dye was distributed more than 1500 μm away from the infusion site. After dye equilibration, differences in dye distribution could be seen in

the various brain regions. However, differences in dye concentration do not affect diffusion measurements because fluorescence recovery after photobleaching is strictly independent of dye concentration. Prior data have shown significant differences in wild-type *vs.* AQP4 null mice in their response to effectors of brain swelling (Manley 2000). Figure 10B shows slowed FITC-dextran diffusion in brain cortex as well as in deep brain structures after hyponatraemia produced by acute water intoxication (10% body weight, i.p.), a well-established model of cytotoxic brain edema. Water intoxication caused progressive slowing of FITC-dextran diffusion in the brain cortex of wild-type mice, with less slowing seen in AQP4 null mice. Remarkably, there was 12-fold slowing of FITC-dextran diffusion 10 min after water

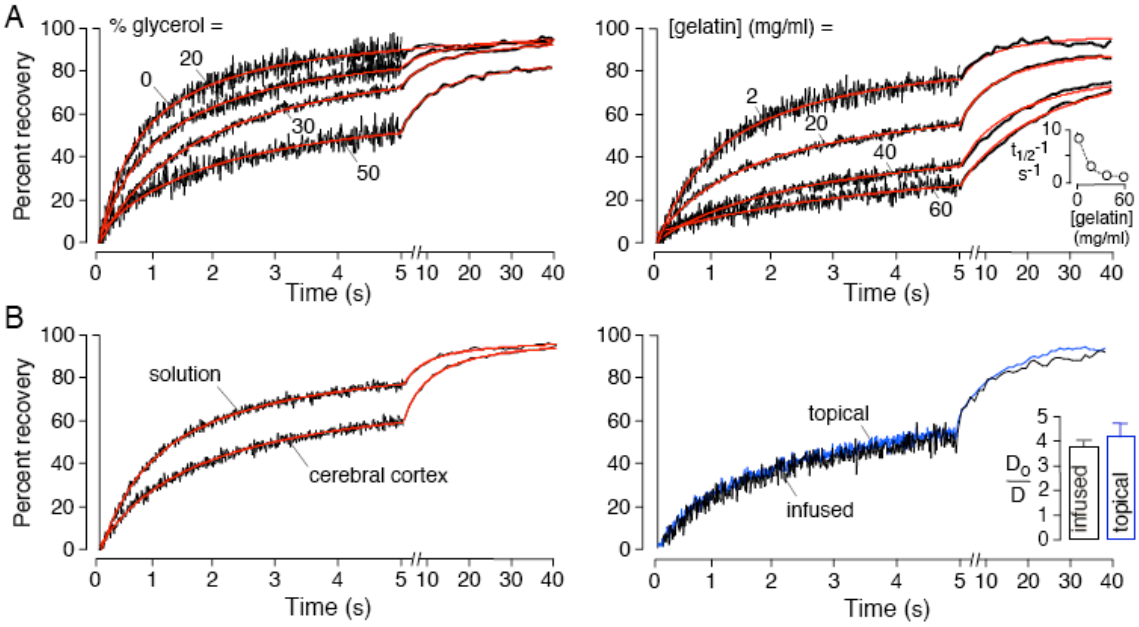

Figure 9. *In vitro* validation of diffusion measurement by microfiberoptic photobleaching. *A*) Photobleaching recovery curves for aqueous glycerol solutions containing 70-kDa FITC-dextran. Original fluorescence recovery data (black) shown as an average of six sets, together with fitted curves (red). Data were fitted by a single-component diffusion model as described in the Materials and Methods section. *B*) Recovery curves from gels consisting of different concentration of gelatin (2–60 mg/ml). Inset shows diffusion rates (reciprocal *t*1/2 values) as a function of gelatin concentration. *C*) Photobleaching recovery curves of FITC-dextran in aCSF (*t*1/2=1.25±0.05 s) and at 400 µm depth (*t*1/2=4.1±0.3) in brain cortex. *D*) Recovery curves at 400 µm depth in brain cortex after surface (topical) application of FITC-dextran (*t*1/2=4.2±0.5 s) *vs.* infusion (*t*1/2=3.8±0.1 s). Inset shows relative dye diffusion in aCSF *vs.* brain tissue (*Do*/*D*) (sd, *n*=4, difference not significant).

intoxication at a depth of 400 µm in cortex of wild-type mice, whereas in AQP4 null mice diffusion did not show significant changes (Figure 10B *right*).

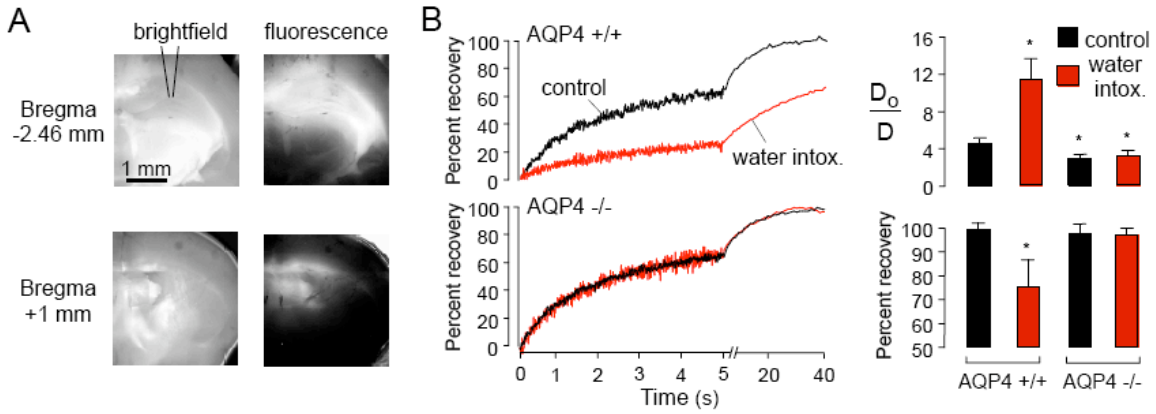

Figure 10. The effect of water intoxication of diffusion in brain ECS. A) Reflected light (left) and fluorescence (right) photographs of brain slice immediately after dye loading by infusion. Top and bottom panels show cross sections at bregma 2.46 and 0 mm, respectively. Overlay shows injection site at 1.4 mm lateral to midline. *B*) Left: recovery curves acquired in cortex (depth 400 m), at 10 min after i.p. injection of 10% body weight saline (control, black) or water (water intox, red) in AQP4 +/+ (top panel) and AQP4 -/- (bottom panel) mice. Right: averaged *Do*/*D* and percentage recovery (avrg±sd, *n* =4, **P*< 0.01, compared with control)

R.2 The function of AQP4 in the development of cytotoxic brain edema following focal cerebral contusion.

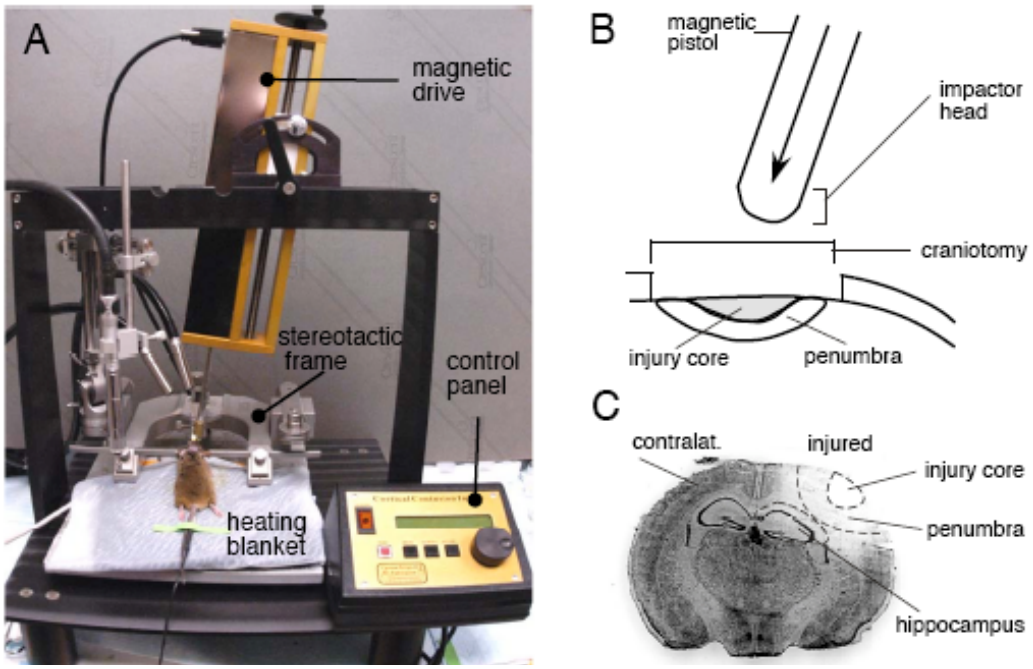

Figure 11: Controlled cortical impact: experimental setup and characterization of the model. A: The mouse cranium is mounted on to a a stereotactic frame and a magnetic pistol -mounted onto a metal frame- is targeted at desired site of injury. The impact velocity, depth and dwell time are set by control panel of the impactor device. B: Schematic of the craniotomy, injury core and penumbra. C: Coronal section of a cresyl violet stained brain, 3 days post injury. Unstained area corresponds to injured tissue, that is subdivided into injury core and penumbra.

Work at our laboratory has shown reduced injury volume, reduced brain water content and improved functional outcome in mice lacking AQP4 using a well-established model of focal cerebral injury (controlled cortical impact). (Figure 11)

Our next aim was to explore the role of AQP4 in the collapse of cerebral microcapillaries long described following brain trauma. We examined brain ultrastructure wild type and AQP4 deficient mice at the previously observed time point of maximal brain water content: 6 hours following impact. As expected, the injury core showed diffuse cellular destruction with extensive necrosis in both groups (data not shown). In the penumbra, there was a considerable swelling of astrocytic perivascular foot processes in the wild type mice (Figure 12).

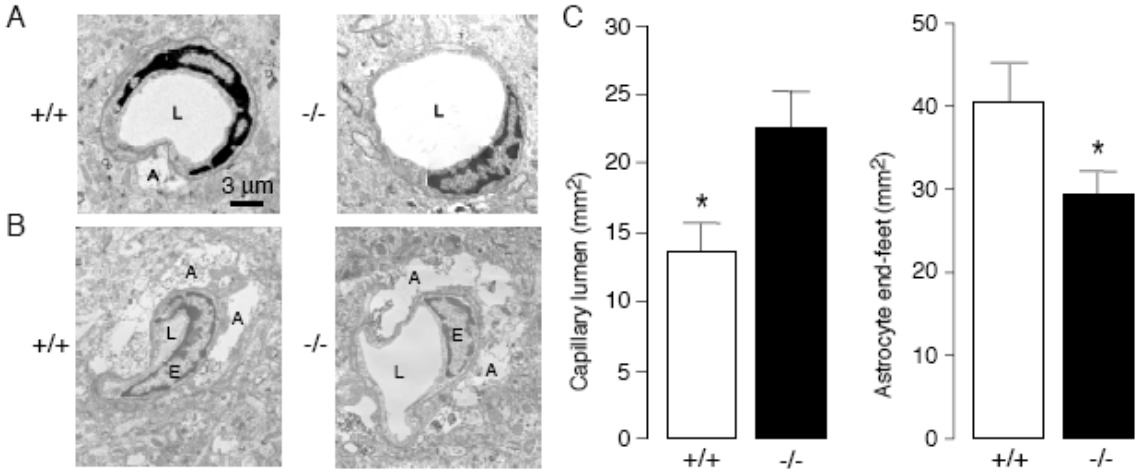

Figure 12: Ultrastructural changes in the injury penumbra. Samples taken at the time point of maximal water content -6 hours following injury. A: Control hemispere, the neurovascular unit structure (endothelial cell, astrocyte foot process) is undistinguishable in AQP4+/+ and AQP4-/- mice. B: Reduced perivascular astrocyte swelling and maintained capillary lumen in AQP4-/- vice relative to AQP4+/+ mice. C: Bargraph depicting data for capillary lumen and astrocyte end feet area shown in B. (S.E., n=11, * $p < 0.05$)

In contrast, significantly less astrocytic swelling was seen in *Aqp4* $^{-/-}$ mice as measured by foot process area (Figure 12, foot process area: 40±5 µm^2 in wild-type versus 29±2 µm^2 in *Aqp4* $^{-/-}$ mice). Swelling of the foot processes compressed the capillary and reduced the lumen diameter. Accordingly, the capillary lumen areas were significantly reduced in wild type mice, compared to a lesser degree of lumen constriction in the AQP4-/- mice (13 ± 2 µm^2 vs. 22 ± 3 µm^2).

R.3 The effect of frequent mutations in the AQP4 gene on water channel permeability.

We created transfected cells expressing reference and variant AQP4 for use in a water permeability assay (Figure 13). As aquaporins are membrane proteins, their degree of expression and localization to the membrane would likely affect water permeability. We examined whether the five nsSNPs affected protein expression and localization.

By Western blot with an AQP antibody, we confirmed AQP4 expression by detecting a ~36kDa band corresponding to the protein, and faint accessory bands representing glycosylated AQP4, as has been observed by others (Figure 13 A, lanes

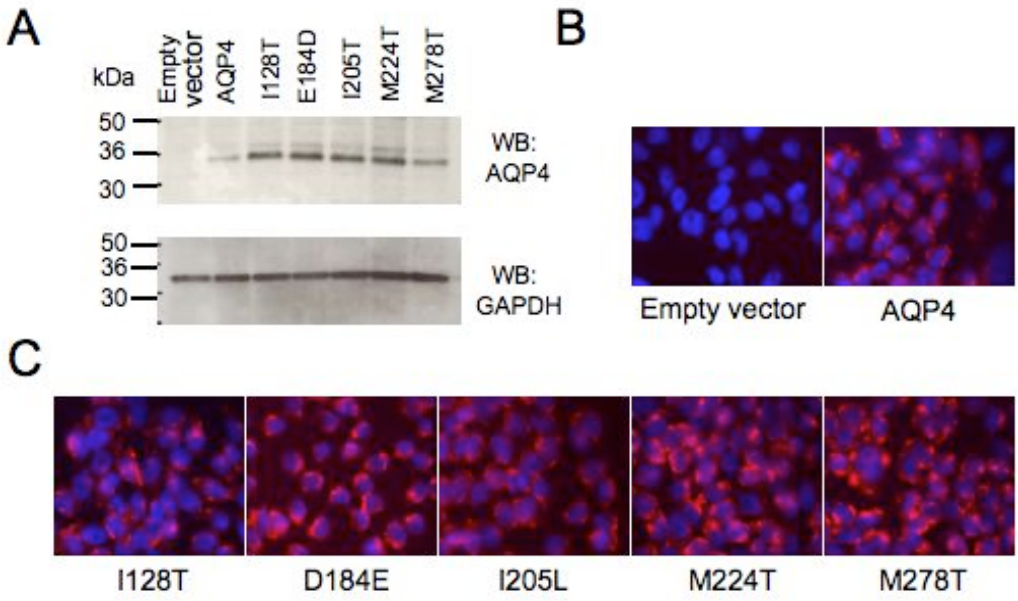

Figure 13: Expression of AQP4 mutants in CHO cell lines. A: Western blot demonstrating ~32 kDA protein bands corresponding to AQP4, GAPDH served as loading control. Immunohistochemistry demonstrating the expression of AQP4 in cell membranes. (B and C).

3-7). We found that most of the protein for reference (wild type AQP4) and mutant proteins were localized to the plasma membrane as shown by immunhistochemistry (Figure 13 B and C).

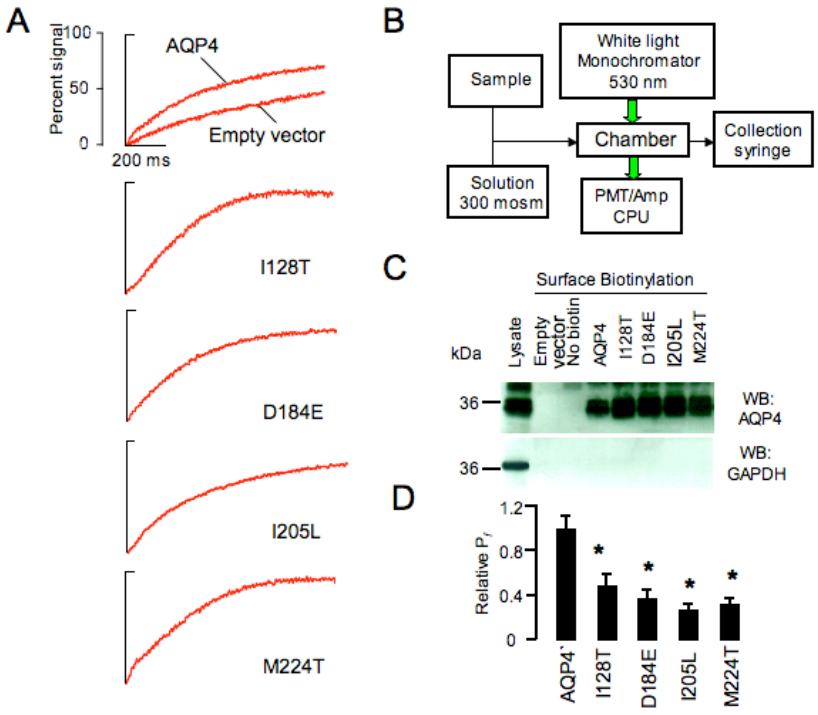

Figure 14. Water permeability of AQP4 variants. A) Original light scattering curves CHO cell suspensions, expressing different AQP4 mutants. B) Schematic of the light scattering experiments. C) Wester blots of cell surface biotinylation probed for AQP4. D) Relative water permeability calculated from the individual t1/2 normalized to the cell surface AQP4 expression. I128T, D184E, I205L and M224T had lower water permeability relative to reference, reduced to 48.3% ± 11.5%, 36.3% ± 8.1%, 25.6% ± 5.8%, and 31% ± 5.6% respectively ($p<0.001$).

The total protein expression levels assessed by Western blot were comparable among reference and mutant proteins (Figure 13 A). To control for loading, blots that were stripped and reprobed for the intracellular enzyme GAPDH showed no signal differences in each sample. We next assessed the effects of the nsSNPs on protein function by measuring water permeability using a cell swelling assay (Verkman et al 1989; van Hoek et al, 1992) where the suspension of cells are subjected to an osmotic challenge and the dynamics of cell swelling is followed based on the change in light scattering of the cell suspension. The measurements resulted in swelling curves as shown in (Figure 14 A).

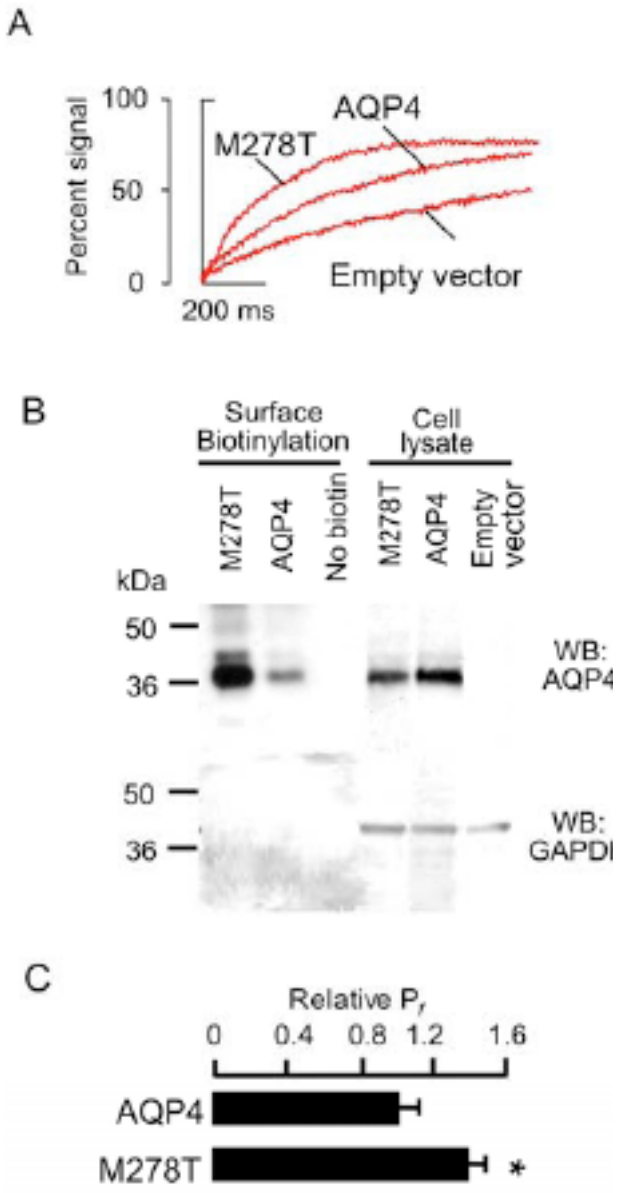

Figure 15. Increased water permeability in the AQP4 M278T variant. A) representative light scattering curve for the CHO cell suspensions transfected with the empty vector, AQP4 and the M278T variant. B) Western blots quantifying surface protein expression of AQP4 M278T. C) Relative water permeability calculated from the individual t1/2 and normalized cell surface AQP4 expression. The M278T variant showed increased relative water permeability (138.1 ± 9.0%, $p<0.001$).

The measurement procedure is represented in Figure 14 B. From the curves we identified the $t_{1/2}$ by fitting the curve to a single exponential equation. Permeability was calculated based on $t_{1/2}$ as described previously (Verkman 2000) with modifications by incorporating cells surface protein concentration (assessed by cell surface biotinylation: Figure 14 C) into our calculations. Cells transfected with reference and all mutant proteins swelled significantly faster than untransfected cells, as expected. Previous work has shown that AQP protein

expression directly correlates with the overall water permeability of the cell membrane (Yang et al, 1997). To take this into account, we calculated relative water permeability by normalizing the permeability against values of cell surface AQP4 protein quantified by cell surface biotinylation (Figure 14 C). We found that the nsSNPs found in our cohort (I128T, D184E, I205L and M224T) had lower relative water permeability, reduced to 48.3% ± 11.5%, 36.3% ± 8.1%, 25.6% ± 5.8%, and 31% ± 5.6% of reference AQP4 respectively ($p<0.001$ for each) (Figure 14 D). Interestingly, the variant predicted by SIFT to be most deleterious, based on evolutionary conservation, was I205L which did in fact produce the greatest reduction in water permeability ($p<0.001$). On the other hand, the previously reported M278T variant in the C-terminal domain showed similar expression and localization and increased relative water permeability (138.1 ± 9.0%, $p<0.001$) (Figure 15).

R.4 Astrocyte swelling in seizures is related to altered GJ phosphorylation.

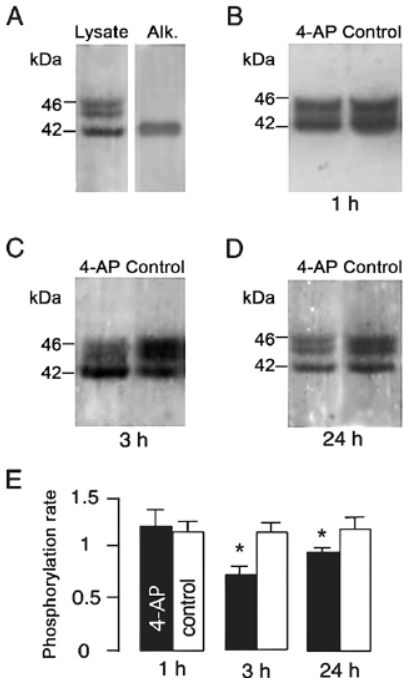

Figure 16. Expression of connexin 43 protein in the cerebral cortex following brief acute seizures. (A) Representative blots demonstrating the phosphorylation- dephosphorylation of connexin 43 isoforms. The P2 (46 kDa), P1 (44 kDa) and non-phosphorylated (NP, 42 kDa) forms were were detected in the control lysate (left), whereas only the NP form was present (right) following alkaline phosphatase treatment (Alk.). (B-D) Original blots demonstrating expression of the phosphorylated and non-phosphorylated forms of connexin 43 at 1 (B), 3 (C) and 24 h (D) following seizure induction. Dephosphorylation is visible at 3 and 24 h in convulsing animals (4-AP) compared to controls. (E) Summarised data of the changes in the phosphorylation of connexin 43 following seizures. Note the decrease in phosphorylation rate at 3 h, which remains significant at 24 h. 4-AP, convulsing animals; control, animals injected with saline; means °æ STDEV, n=5, p=0.0017 at 3 h; $p<0.01$ at 24 h.

Using a well-established model of brief acute seizures, we followed the expression of the astrocyte specific GJ protein connexin 43 on western blot (Figure 16). The different forms of connexin 43 were identifiable based on their different migration: the two phosphorylated forms, P1 and P2, migrated at 44 kDa and 46 kDa, respectively, while the non-phosphorylated protein (NP) was detected at 42 kDa. The phosphorylation status of the identified forms was confirmed with digestion of samples with alkaline phosphatase that produced a single NP band (insert). The

phosphorylation status of connexin 43 was unchanged at 1 h (Figure 15B), but at 3 h (Figure 15C) following 4-AP treatment there was an ~50% decrease (p=0.0017) in the ratio of phosphorylated versus non-phosphorylated connexin 43 forms in the epileptic animals. Surprisingly, this dephosphorylated status persisted until 24 h post seizure as a significant ~10% reduction in phosphorylation.

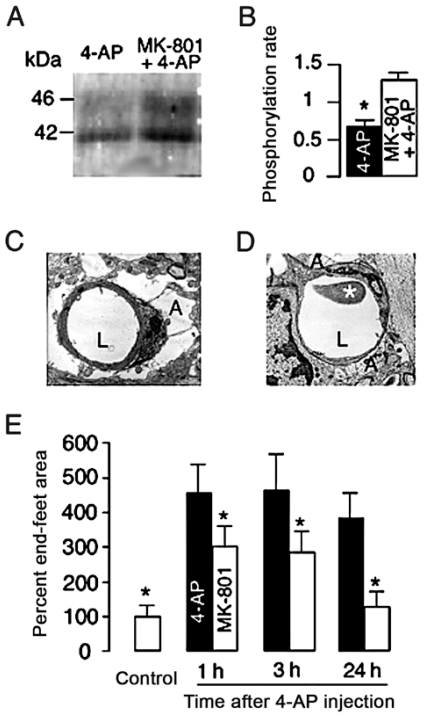

Figure 17. Connexin 43 dephosphorylation (A and B) and seizure-associated glial swelling (C and D) in the cerebral cortex can be reversed by MK-801 pre-treatment. (A) Representative blots showing the strong presence of phosphorylated connexin 43 after MK-801 pre-treatment 3 h following seizure induction. (B) Summarised data from panel A blots (n=5; p<0.01). (C and D) Representative electron micrographs demonstrating perivascular glial swelling at 3 h post seizure induction (C), and reduced by MK-801 pretreatment (D). A, astrocyte end-feet; L, capillary lumen; asterisk, red blood cell. (E) Graph summarising percent changes in astrocytic end-feet area at 1, 3 and 24 h post 4-AP injection. Note the prolonged swelling, significant at 1, 3 and 24 h, and the protective effect of MK-801 (average °æ STDEV, n=27-33; p<0.001).

To clarify the relation between NMDA receptor activation in 4-AP seizures and the subsequent phosphorylation changes of connexin 43, the NMDA antagonist MK-801 was applied prior to seizure induction. This pre-treatment resulted in a decrease in connexin 43 dephosphorylation at 3 h (Figure 17A and B), suggesting that the long-lasting seizure effect was the result of NMDA-dependent mechanism. To relate the phosphorylation status of Cx 43 to cell swelling, in our next experiment we measured the area of perivascular astrocyte processes at baseline, following 4-AP seizures with and without MK-801 pre-treatment was measured (Figure 17C and D). Baseline values of the astrocytic end-feet area in untreated animals were considered to be 100% for the purposes of our analysis. A 464% ± 85 increase in the size of the end-feet compared to baseline was seen at 1 h following seizure induction, followed by a 471% ± 104 and 392% ± 71 increase in size at 3 and 24h, respectively (n=29-34, p<0.001). Swelling was abolished by the application of MK-801 with 310% ± 59, 292% ± 59 and 129% ± 45 end-feet areas in the 1, 3, and 24 h groups, respectively (n=28-32, p<0.001) (Figure 16 E), which essentially parallels gap junction phosphorylation status.

Discussion

Our study demonstrates novel mechanisms in the development of cytotoxic edema. We show the importance of *gap junctions* and *AQP4 variants* in cytotoxic cell swelling. Furthermore, we provided new evidence that two factors of cerebral edema development, the *microcapillary compression* and *slowed ECS diffusion* are results of AQP4 dependent astrocyte swelling.

D.1 Slowed ECS diffusion is related to AQP4 dependent astrocyte swelling.

The swelling of CNS cells in cytotoxic brain edema takes place at the expense of brain extracellular space (Hrabetova et al, 2003; Kume-Kick et al, 2002; Binder et al, 2004; Zador et al, 2008). Such contraction of brain ECS result in the impaired diffusion of ions, metabolites, macromolecules and drugs. Osmotically induced swelling in slices demonstrated a linear relationship between the reduction of extracellular space volume fraction (percent of brain tissue volume occupied by the extracellular space) and the solution osmolarity in hyposmotic condition (Kume-Kick et al, 2002). In vivo measurements show the baseline value of ECS fraction to be ~20%, which dramatically decreases during pathologies such as prolonged seizure (Binder et al, 2004), cortical spreading depression (van Harreveld and Khattab, 1967) as well as cytotoxic edema. The current methods are only capable of measuring the diffusion of TMA, a biologically irrelevant ion in deeper cortical layers and do not grant the option to follow the movement of fluorescently labeled macromolecules such as dextrans. Recent methodological advances granted the option of following diffusion of FITC tagged macromolecules in superficial cortical layers (Binder et al, 2004; Thorn and Nicholson 2006) using integrated optic imaging (IOI) or the technique of surface photobleaching respectively. Here we present a new method using microfiber optic, that allows measurement of macromolecular diffusion in deep brain structures. Our results show a marked impairment of diffusion in cytotoxic brain edema with dextrans, in accordance with previous studies of TMA and IOI. Our results also show that delayed cell swelling seen in AQP4 deficient mice translate into a delayed slowing/preservation of ECS diffusion in the deep layers of the cerebral cortex. These results imply, that similarly to superficial layers of the cortex the deletion of AQP4 helps maintain extracellular diffusion in cytotoxic edema by impairing astrocyte swelling. Another benefit of the current method is that it grants access to deep brain structures and as such could be used in studying the relation of

ECS changes in seizures, cortical spreading depression and other neuroexcitatory processes in areas such as the hippocampus or basal ganglia. Another utilization of the method is studying the structure of deep tumors or other focal pathologies in the brain parenchyma.

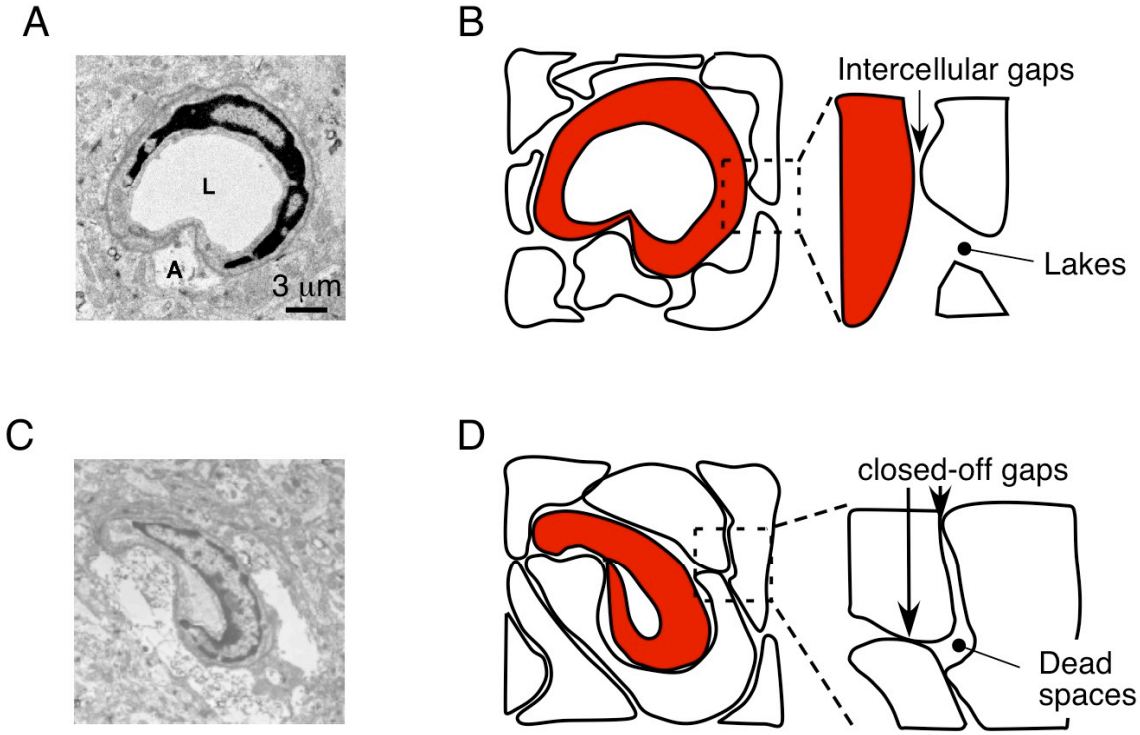

Figure 18: The role of AQP4 in two mechanisms related to cytotocxic brain edema. The contraction of extracellular space and the compression of microcapillaries is a result of AQP4 dependent astrocyte end feet swelling, proven using a transgenic mouse model in Aims 1 and 2. A, B: Baseline ultrastructure and overlay schematic demonstrating open intercellular space gaps and lakes as well as a patent capillary lumen. C and D: Closed ECS (assessed by FRAP method in the current thesis) and collapsed microcapillary.

D2. Microcapillary compression is related to AQP4 dependent astrocyte swelling.

Our experiments encompass another effect of astrocyte swelling, which is less anticipated by our clinical thinking. The perivascular astrocytic foot processes have been demonstrated as the predilectional site of swelling in cytotoxic edema. Interestingly enough, this happens to be the locus of polarized AQP4 expression. The structural molecule alpha syntrophin has been shown to anchor AQP4 at this site (Amiry-Moghaddam et al, 2004a; Bragg et al, 2006; Neely et al, 2001). The deletion of alpha syntrophin results in the depolarization of AQP4 channel (Amiry-Moghaddam et al, 2004b) as shown by immunogold electron micrographs. Subsequent studies have show the mice lacking alpha syntrophin to be phenotypical equivalents of AQP4 deficient mice, underlining the importance of the polarized expression of AQP4 at astrocyte end feet.

Using transmission electron microscopy, we demonstrated the swelling of perivascular astrocytes and their compression of microcapillaries in the penumbra of a focal cortical injury, 6 hours following the impact. In parallel experiments, matching AQP4 deficient mice showed reduced perivascular astrocyte swelling, in accordance with experiments of cytotoxic edema (Manley et al, 2000). Concomitantly, we found the significant decrease of microcapillary compression in AQP4 deficient mice compared to wild-type littermates.

We demonstrated AQP4 to be responsible for the microcapillary compression described in cerebral edema. The relevance of this finding is that in addition to astrocyte foot process swelling, the development of cytotoxic brain edema is known to be paralleled by the progressive reduction of cerebral blood flow (Yamaguchi et al, 1994). Another set of experiments demonstrated that in moderate levels of cytotoxic edema CBF is reduced independent of ICP (Meinig et al, 1973), suggesting that microvascular compression increases the resistance of the cerebral vasculature and as such it impaired CBF independently of ICP elevation that opposed CPP. Therefore interventions inhibiting AQP4 function could help augment CBF in brain edema.

D3. Frequent variants of AQP4 modulate osmotic cell swelling

Cytotoxic brain swelling is present in early ischemic stroke and brain trauma, as well as metabolic disturbances and water intoxication. The major discrepancy between the extent of ischemic or traumatic brain injury and the accompanying clinical picture is a puzzle encountered in every day medical practice. This introduces difficulties in predicting clinical outcome as well as choosing the therapeutic protocol in the treatment. Recent results illuminated variations in the AQP4 gene as a cause of the diverse clinical course in malignant MCA strokes (Kleffner et al, 2008) and cerebral trauma (Romeiro et al, 2007). But till now, none of the studies have tested the functional impact of AQP4 variants on channel water permeability. Our current study identified and tested the function of single nucleotide polymorphisms (SNPs) of AQP4. Water permeability was reduced in four of the variants, while one mutation resulted in enhanced water transport. Using cell surface biotinylation experiments, we found increase in the membrane pool of this latter variant suggesting the reduction of protein turnover. The role of AQP4 is on one hand to facilitate the development of cytotoxic edema, but on the other hand, to help the clearance (decrease) of vasogenic edema. We may need to include the functional significance of AQP4 variants into our clinical thinking and management of cerebral edema, and we also need to separate the binary effects of AQP4 in specific brain pathologies.

D4. Modulation in gap junction phosphorylation is associated with cytotoxic astrocyte swelling following seizures

Diffusion Weighted Imaging demonstrated slowed diffusion following seizures and subsequent electron microscopy showed widespread astrocyte swelling which is considered to be the hallmark of cytotoxic brain edema. The metabolic burden of an epileptic seizure together with the release of neurotransmitters and ions such as potassium create an osmotic drive for water to enter the cell and result in swelling. A line of studies demonstrated the high water permeability of astrocytes first in vitro (Solenov et al, 2004; Yang et al, 1997), and most recently in vivo two-photon microscopy has shown rapid swelling of astrocytes in hyposmotic conditions (Nase et al, 2008). Astrocytes harbor numerous ion transport mechanisms to regulate their volume (Chen et al, 2005; Kimelberg et al, 2006) and compensate for pathological volume changes. Evidence suggests that they do not only function as individual units in compensating cytotoxic swelling, but also as a cellular network that traffics ions and neurotransmitters via low resistance intercellular GJs. (Wallraf et al, 2006). The regulatory decrease in the phosphorylation rate of GJ subunit connexin 43 has been demonstrated in conditions reconstituting a seizure-like environment (high K and glutamate) (Nagy et al, 2000), which also resulted in the decrease of cellular coupling. Our present study is the first to demonstrate the dephosphorylation of connexin 43 in parallel with cytotoxic astrocyte swelling. Based on this we propose, that the closure of intercellular gap junctions essentially isolates individual astrocytes and thus impairs compensatory water trafficking out of the swollen cells via the astrocyte network. From This observation further emphasizes the role of gap junction protein, connexin 43 in cytotoxic brain edema and in facilitating the related compensatory mechanisms of ion and water transport.

Conclusion

Astrocyte network in cytotoxic edema is related to the dysfunction of their multi cellular networks, which results in impaired ECS diffusion and cerebral microcirculation (Figures 19, 20)

The current thesis uncovers new mechanisms of cerebral edema: that the long described phenomenon's of brain extracellular space contraction and microcapillary compression is a result of AQP4 dependent astrocyte swelling (Figure 18). We also introduced new cellular concepts regarding the mechanisms of cytotoxic brain edema: the contribution of regulatory changes in gap junction protein connexin 43, and variants of AQP4 both impact astrocyte swelling. Based on our results we also demonstrate the validity of the concept of the astrocytic network acting as a functional syntitium in trafficking water in cerebral edema (Figure 19).

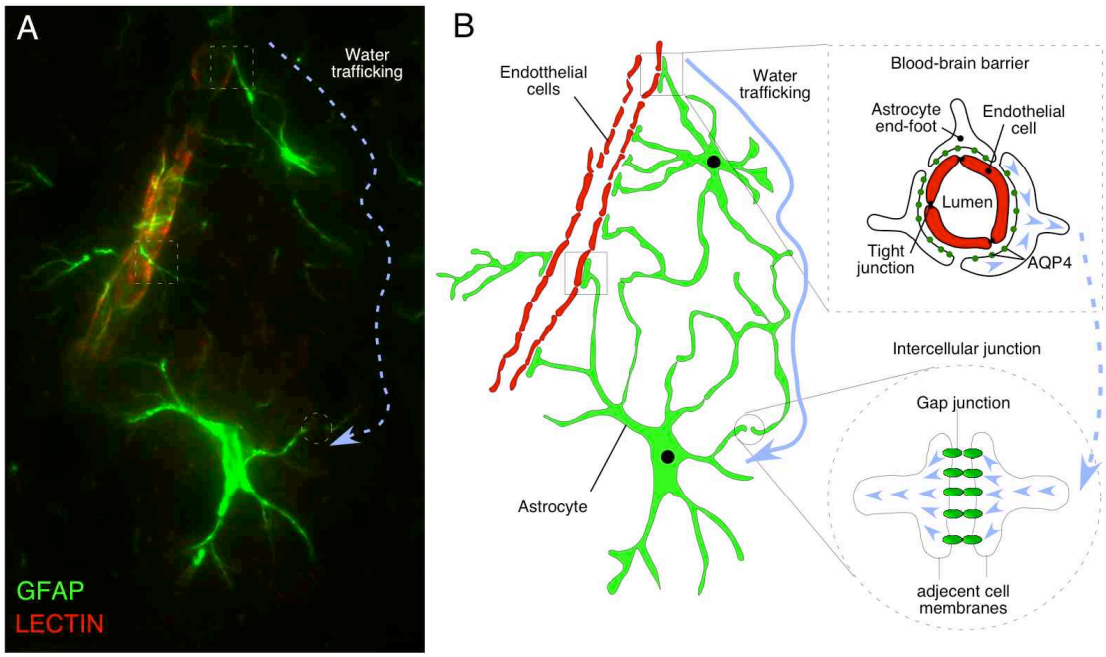

Figure 19: Astrotyes act as a multicellular unit (cellular network) in the development of cytotoxic edema (Aims 3 and 4): the concept of serial water trafficking interfaces of astrocytes consisting of AQP4 (BBB interface) and gap junctions (intercellular interface). A: fluorescent stain (Zador non-published) detecting astrocytes (GFAP stain) and the capillary bed (lectins stain). Note the perivascular processes hugging the capillary lumen and the arborization of astrocyte processes interconnecting adjacent cells. B: Overlay schematic of "A" (left) with blue continuous arrow outlining the theoretical flow of water through the cellular network. Insets demonstrating the polarization of AQP4 at perivascular foot processes of the blood-brain barrier (*right top*) and the intercellular junction of astrocytes (*right bottom*). Blue arrows and interrupted blue line defines the direction of water flow across the cell membrane.

These findings help us tailor our current view of cerebral edema in two main aspects: 1) the development of cerebral edema is likely to be enhanced by a) altered aquaporin 4 permeability due to single nucleotide polymorphisms, b) closure of gap junction due

to dephosphorylation. 2) The astrocyte swelling related to these functional changes are A: impaired diffusion of macromolecules/drug carriers deep in brain, B: impair cerebral perfusion due to microcapillary compression. Our current therapeutic thinking should therefore consider: 1) detecting AQP4 variants in head trauma patients, 2) modulate gap junction function 3) the employment of small molecular carriers that penetrate contracted ECS 4) the use of artificial small oxygen carriers that pass through the compromised capillaries (Figure 20).

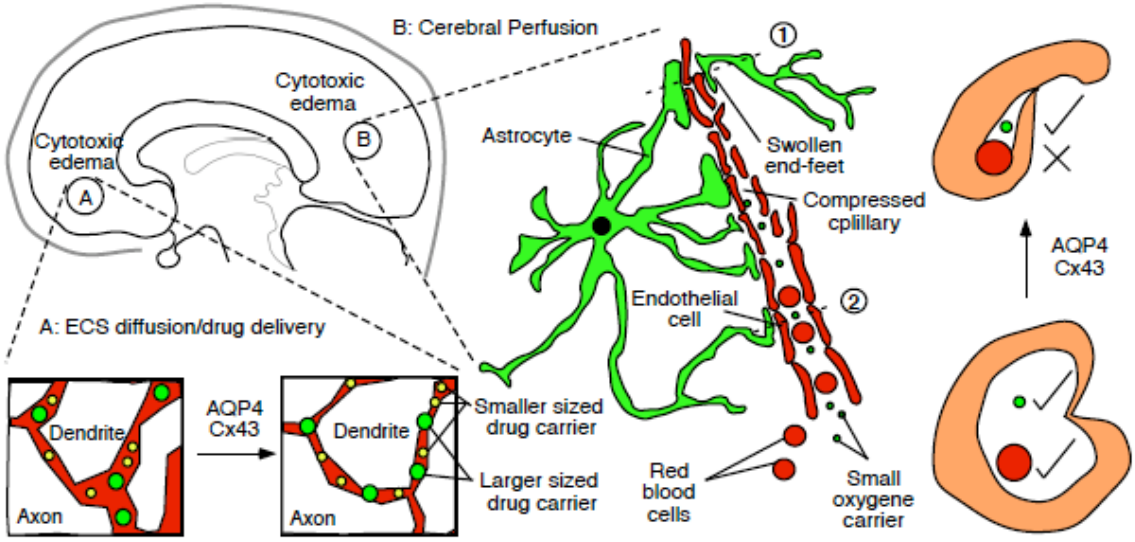

Figure 20. Therapeutic relevances of the current thesis. The astrocyte swelling related to AQP4 and Cx 43 translates into A: impaired diffusion in brain due to ECS contraction, which implies the use of small drug carriers versus larger ones (left inset; physiological condition, right inset cytotoxic edema) B: Impaired cerebral perfusion due to microcapillary compromise, suggests the employment of small oxygen carriers. (bottom inset (2); physiological condition, top inset (1) cytotoxic edema)

Acknowledgements

I would like to thank Professor András Mihály at the Department of Anatomy, University of Szeged for tutoring me during my undergraduate years and through various steps of my work as PhD student. Professor Geoffrey Manley, chief of neurotrauma for his tutorship and for introducing me to an intense and fruitful research environment at his laboratory at the University of California San Francisco, Department of Neurosurgery. I feel that this exposure has contributed a most valuable part of my training in translational research and also fortified my interest in neuroscience. My coworkers Dr. Daniel Lu, Dr. Mazin Magzoub, Mr Marios Papadopoulos, and Dr. Xiaoming Yao for their technical help, and their collegiality. Professor Pál Barzó from the Department of Neurosurgery, University of Szeged for his support and allowing me leave for my research. Professor Michael Lawton chief of vascular neurosurgery at UCSF Department of Neurosurgery and his chief resident Dr. Daniel Lu for their teaching, inspiration, professional support, and also for greatly augmenting my interest and training in operative neurosurgery.

For their technical help, I would like to thank Professors Bernard Himpens, Johan Vereecke and Dr. Marie Malfait from the Laboratory of Physiology, KU Leuven, Belgium for providing us with the connexin 43 antibody. Dr. Andrea Bagosi for her help with the EM measurements.

Finally, I whish to thank my family and friends for their patience and support. Sorry for being away for such a long time.

References

Adrogué HJ, Madias NE. 2000. Hyponatremia. N Engl J Med. 342:1581-9.

Agre, P, King, LS, et al. 2002. Aquaporin water channels: from atomic structure to clinical medicine. J. Physiol. 542: 3–16.

Alexander,JJ, Bao L, JacobA, Kraus DM, Holers VM, Quigg RJ. 2003. Administration of the soluble complement inhibitor, Crry-Ig, reduces inflammation and aquaporin 4 expression in lupus cerebritis. Biochim. Biophys. Acta, 1639:169-176.

Amiry-Moghaddam M, Frydenlund DS, Ottersen OP. 2004a. Anchoring of aquaporin-4 in brain: molecular mechanisms and implications for the physiology and pathophysiology of water transport. Neuroscience. 129:999-1010.

Amiry-Moghaddam M, Xue R, Haug FM, Neely JD, Bhardwaj A, Agre P, Adams ME, Froehner SC, Mori S, Ottersen OP. 2004b Alpha-syntrophin deletion removes the perivascular but not endothelial pool of aquaporin-4 at the blood-brain barrier and delays the development of brain edema in an experimental model of acute hyponatremia. FASEB J. 2004 Mar;18(3):542-4.

Axelrod D, Koppel DE, Schlessinger J, Elson E, Webb WW. 1976. Mobility measurement by analysis of fluorescence photobleaching recovery kinetics. Biophys J. 16:1055-69.

Badaut J, Lasbennes F, Magistretti PJ, Regli L. 2002. Aquaporins in brain: distribution, physiology, and pathophysiology. J Cereb Blood Flow Metab 22:367-78.

Barzó P, Marmarou A, Fatouros P, Hayasaki K, Corwin F. 1997. Contribution of vasogenic and cellular edema to traumatic brain swelling measured by diffusion-weighted imaging. J Neurosurg. 1997 87:900-7.

Behan LA, Phillips J, Thompson CJ, Agha A. 2008. Neuroendocrine disorders after traumatic brain injury. J Neurol Neurosurg Psychiatry. 79:753-9.

Binder DK, Yao X, Verkman AS, Manley GT. 2006. Increased seizure duration in mice lacking aquaporin-4 water channels. Acta Neurochir Suppl. 96:389-92.

Binder DK, Papadopoulos MC, Haggie PM, Verkman AS. 2004. In vivo measurement of brain extracellular space diffusion by cortical surface photobleaching. J. Neurosci. 24:8049–8056.

Bloch O, Papadopoulos MC, Manley GT, Verkman AS. 2005. Aquaporin-4 gene deletion in mice increases focal edema associated with staphylococcal brain abscess. J Neurochem. 95:254-62.

Bourke RS, Kimelberg HK, Nelson LR, Barron KD, Auen EL, Popp AJ, Waldman JB. 1980. Biology of glial swelling in experimental brain edema. Adv Neurol. 28:99-109.

Bragg AD, Amiry-Moghaddam M, Ottersen OP, Adams ME, Froehner SC. 2006. Assembly of a perivascular astrocyte protein scaffold at the mammalian blood-brain barrier is dependent on alpha-syntrophin. Glia. 53:879-90.

Brain Trauma Foundation; American Association of Neurological Surgeons; Congress of Neurological Surgeons; Joint Section on Neurotrauma and Critical Care, AANS/CNS, Bratton SL, Chestnut RM, Ghajar J, McConnell Hammond FF,

Harris OA, Hartl R, Manley GT, Nemecek A, Newell DW, Rosenthal G, Schouten J, Shutter L, Timmons SD, Ullman JS, Videtta W, Wilberger JE, Wright DW. 2007. Guidelines for the management of severe traumatic brain injury. VIII. Intracranial pressure thresholds. J Neurotrauma. 24:S55-8.

Chen H, Sun D. 2005. The role of Na-K-Cl co-transporter in cerebral ischemia. Neurol Res. 2005 27:280-6.

Chomczynski P and Sacchi N. 1987. Single-step method of RNA isolation by acid guanidinium thiocyanate-phenol-chloroform extraction. Anal Biochem 162:156-159.

Christ GJ, Day NS, Day M, et al, 2003. Increased connexin43-mediated intercellular communication in a rat model of bladder overactivity in vivo. Am J Physiol Regul Integr Comp Physiol 284: R1241-R1248.

Condorelli DF, Trovato-Salinaro A, Mudo G, Mirone MB and Belluardo N. 2003. Cellular expression of connexins in the rat brain: neuronal localization, effects of kainate-induced seizures and expression in apoptotic neuronal cells. Eur J Neurosci 18: 1807-1827.

De Sousa PA, Valdimarsson G, Nicholson BJ and Kidder GM. 1993. Connexin trafficking and the control of gap junction assembly in mouse preimplantation embryos. Development 117: 1355-1367.

Diamond MC, Scheibel AB, Murphy GM Jr, Harvey T. 1985. On the brain of a scientist: Albert Einstein. Exp Neurol. 88:198-204.

Duffy HS, Fort AG, Spray DC. 2006. Cardiac connexins: genes to nexus. Adv Cardiol. 42:1-17.

Fabene PF, Weiczner R, Marzola P, et al. 2006. Structural and functional MRI following 4-aminopyridine-induced seizures: a comparative imaging and anatomical study. Neurobiol Dis 21: 80-89.

Fishman, R.A. 1975. Brain edema. N. Engl. J. Med., 293: 706–711.

Flagg-Newton J, Simpson I, Loewenstein WR. 1979. Permeability of the cell-to-cell membrane channels in mammalian cell juncton. Science 205: 404-407.

Fort P, Marty L, Piechaczyk M, et al. 1985. Various rat adult tissues express only one major mRNA species from the glyceraldehyde-3- phosphate-dehydrogenase multigenic family. Nucleic Acids Res 13: 1431-1442.

Franklin, K. B. J., and Paxinos, G. 1997. The Mouse Brain in Stereotaxic Coordinates, 2nd Ed., Academic Press, New York

Fu X, Li Q, Feng Z, Mu D. 2007. The roles of aquaporin-4 in brain edema following neonatal hypoxia ischemia and reoxygenation in a cultured rat astrocyte model.

Glia. 55:935-41.

Goldberg GS, Valiunas V and Brink PR. 2004. Selective permeability of gap junction channels. Biochim Biophys Acta 1662: 96-101.

Greenberg MS. 2006 Handbook of neurosurgery 6th edition, Thieme New York

Hackett PH, Roach RC. 2001. High-altitude illness. N Engl J Med. 345:107-14.

Hara,H. and Shibuya,S. 2002. Reduced aquaporin 4 expression in the muscle plasma membrane of patients with Duchenne muscular dystrophy. Arch. Neurol., 59, 431-437.

Hardin JA, Wallace LE, Wong JF, O'Loughlin EV, Urbanski SJ, Gall DG, MacNaughton WK, Beck PL. 2004. Aquaporin expression is downregulated in a murine model of colitis and in patients with ulcerative colitis, Crohn's disease and infectious colitis. Cell Tissue Res. 318:313-23.

Hemphill JC 3rd, Knudson MM, Derugin N, Morabito D, Manley GT. 2001. Carbon dioxide reactivity and pressure autoregulation of brain tissue oxygen. Neurosurgery 48:377-83.

Hrabetová S, Hrabe J, Nicholson C. 2003. Dead-space microdomains hinder extracellular diffusion in rat neocortex during ischemia. J Neurosci 23:8351-9.

Hypothermia after Cardiac Arrest Study Group. 2002. Mild therapeutic hypothermia to improve the neurologic outcome after cardiac arrest. N Engl J Med. 346:549-56.

Kimelberg HK. 1992. Astrocytic edema in CNS trauma. J Neurotrauma. 9:S71-81.

Kimelberg HK, Barron KD, Bourke RS, Nelson LR, Cragoe EJ. 1990. Brain anti-cytoxic edema agents. Prog Clin Biol Res 361:363-85.

Kimelberg HK, Macvicar BA, Sontheimer H. 2006. Anion channels in astrocytes: biophysics, pharmacology, and function. Glia. 54:747-57.

Kimelberg HK, Rutledge E, Goderie S, Charniga C. 1995. Astrocytic swelling due to hypotonic or high K+ medium causes inhibition of glutamate and aspartate uptake and increases their release. J Cereb Blood Flow Metab. 15:409-16.

Klatzo I. 1967. Presidental address. Neuropathological aspects of brain edema. J Neuropathol Exp Neurol. 26:1-14.

Kleffner I, Bungeroth M, Schiffbauer H, Schäbitz WR, Ringelstein EB, Kuhlenbäumer G. 2008. The role of aquaporin-4 polymorphisms in the development of brain edema after middle cerebral artery occlusion. Stroke. 39:1333-5.

Kovacs A, Mihaly A, Komaromi A, et al. 2003. Seizure, neurotransmitter release, and gene expression are closely related in the striatum of 4-aminopyridine-treated rats. Epilepsy Res 55:117-129.

Kume-Kick J, Mazel T, Vorisek I, Hrabětová S, Tao L, Nicholson C. 2002.

Independence of extracellular tortuosity and volume fraction during osmotic challenge in rat neocortex. J Physiol. 542:515-27.

Lee TS., Eid T, Mane S, Kim JH, Spencer DD, Ottersen OP. de Lanerolle NC. 2004. Aquaporin-4 is increased in the sclerotic hippocampus in human temporal lobe epilepsy. Acta Neuropathol, 108:493-502.

Lu DC, Binder DK, Chien B, Maisel A, Manley GT. 2008. Cerebral salt wasting and elevated brain natriuretic peptide levels after traumatic brain injury: 2 case reports. Surg Neurol. 69:226-9.

Ma T, Yang B, Gillespie A, Carlson EJ, Epstein CJ, Verkman AS. 1997. Generation and phenotype of a transgenic knockout mouse lacking the mercurial-insensitive water channel aquaporin-4. J Clin Invest. 100:957-62.

Malfait M, Gomez P, van Veen TA, et al. 2001. Effects of hyperglycemia and protein kinase C on connexin43 expression in cultured rat retinal pigment epithelial cells. J Mem Biol 181: 31-40.

Manley GT, Fujimura M, Ma T, Noshita N, Filiz F, Bollen AW, Chan P, Verkman AS. 2000. Aquaporin-4 deletion in mice reduces brain edema after acute water intoxication and ischemic stroke. Nat Med. 6:159-63.

Martin PE and Evans WH. 2004. Incorporation of connexins into plasma membranes and gap junctions. Cardiovasc Res 62:378-387.

Mazel T, Richter F, Vargová L, Syková E. 2002. Changes in extracellular space volume and geometry induced by cortical spreading depression in immature and adult rats. Physiol Res. 51:S85-93.

Meinig G, Reulen HJ, Magawly C. 1973. Regional cerebral blood flow and cerebral perfusion pressure in global brain oedema induced by water intoxication. Acta Neurochir (Wien). 29:1-13.

Mihaly A, Bencsik K and Solymosi T. 1990. Naltrexone potentiates 4-aminopyridine seizures in the rat. J Neural Transm Gen Sect 79:59-67.

Mihaly A, Borbely S, Vilagi I, et al. 2005. Neocortical c-fos mRNA transcription in repeated, brief, acute seizures: is c-fos a coincidence detector? Int J Mol Med 15: 481-486.

Musil LS and Goodenough DA. 1991. Biochemical analysis of connexin43 intracellular transport, phosphorylation, and assembly into gap junctional plaques. J Cell Biol 115: 1357-1374.

Nagy JI, Li WE. 2000. A brain slice model for in vitro analyses of astrocytic gap junction and connexin43 regulation: actions of ischemia, glutamate and elevated potassium. Eur J Neurosci 12:4567-4572.

Nagy JI, Rash JE. 2000b. Connexins and gap junctions of astrocytes and oligodendrocytes in the CNS. Brain Res Brain Res Rev. 32:29-44.

Nase G, Helm PJ, Enger R, Ottersen OP. 2008. Water entry into astrocytes during brain edema formation. Glia. 56:895-902.

Neal CJ, Lee EY, Gyorgy A, Ecklund JM, Agoston DV, Ling GS. 2007. Effect of penetrating brain injury on aquaporin-4 expression using a rat model. J Neurotrauma. 24:1609-17.

Neely,JD., Amiry-Moghaddam M, Ottersen OP, Froehner SC, Agre P, Adams ME. 2001. Syntrophin-dependent expression and localization of Aquaporin-4 water channel protein. Proc. Natl. Acad. Sci. USA. 98:14108-14113.

Nemani VM, Binder DK. 2005. Emerging role of gap junctions in epilepsy. Histol Histopathol 20:253-259.

Oyesiku MN, Amacher AL, 1990. Patient Care in Neurosurgery, Lippincott Williams and Wilkins; 3rd Revised edition

Papadopoulos MC, Binder DK, Verkman AS. 2005. Enhanced macromolecular diffusion in brain extracellular space in mouse models of vasogenic edema measured by cortical surface photobleaching. FASEB J. 19:425-7.

Papadopoulos MC, Manley GT, Krishna S, Verkman AS. 2004. Aquaporin-4 facilitates reabsorption of excess fluid in vasogenic brain edema. FASEB J. 18:1291-3.

Papadopoulos MC, Verkman AS. 2005. Aquaporin-4 gene disruption in mice reduces brain swelling and mortality in pneumococcal meningitis. J Biol Chem 280:13906-12.

Qiu C, Coutinho P, Frank S, Franke S, Law LY, Martin P, Green CR, Becker DL. 2003. Targeting connexin43 expression accelerates the rate of wound repair. Curr Biol. 13:1697-703.

Rama Rao KV, Norenberg MD. 2007. Aquaporin-4 in hepatic encephalopathy. Metab Brain Dis. 22:265-75.

Rash, JE, Yasumura T, et al. 1998. Direct immunogold labeling of aquaporin-4 in square arrays of astrocyte and ependymocyte plasma membranes in rat brain and spinal cord. Proc. Natl. Acad. Sci. U.S.A., 95:11981–11986.

Rodríguez-Baeza A, Reina-de la Torre F, Poca A, Martí M, Garnacho A. 2003. Morphological features in human cortical brain microvessels after head injury: a three-dimensional and immunocytochemical study. Anat Rec A Discov Mol Cell Evol Biol. 273:583-93.

Romeiro RR, Romano-Silva MA, De Marco L, Teixeira AL Jr, Correa H. 2007. Can

variation in aquaporin 4 gene be associated with different outcomes in traumatic brain edema? Neurosci Lett. 426:133-4.

Saadoun S, Papadopoulos M, Bell B, Krishna S, Davies D. 2002. The aquaporin-4 water channel and brain tumour oedema. J. Anat. 200:528.

Saez JC, Contreras JE, Bukauskas FF, Retamal MA, Bennett MV. 2003. Gap junction hemichannels in astrocytes of the CNS. Acta Physiol Scand 179:9-22.

Seksek O, Biwersi J, Verkman AS. 1997. Translational diffusion of macromolecule-sized solutes in cytoplasm and nucleus. J. Cell Biol. 138:131–142

Silver IA, Deas J, Erecińska M. 1997. Ion homeostasis in brain cells: differences in intracellular ion responses to energy limitation between cultured neurons and glial cells. Neuroscience. 78:589-601.

Simard M, Nedergaard M. 2004. The neurobiology of glia in the context of water and ion homeostasis. Neuroscience 129:877-896.

Simpson I, Rose B, Loewenstein WR. 1977. Size limit of molecules permeating the junctional membrane channels. Science 195:294-296.

Sinclair C, Kirk J, Herron B, Fitzgerald U, McQuaid S. 2007. Absence of aquaporin-4 expression in lesions of neuromyelitis optica but increased expression in multiple sclerosis lesions and normal-appearing white matter. Acta Neuropathol 113:187-94.

Solenov E, Watanabe H, Manley GT, Verkman AS. 2004. Sevenfold-reduced osmotic water permeability in primary astrocyte cultures from AQP-4-deficient mice, measured by a fluorescence quenching method. Am J Physiol Cell Physiol. 286:C426-32.

Sorani MD, Zador Z, Hurowitz E, Yan D, Giacomini KM, Manley GT. 2008. Novel variants in human Aquaporin-4 reduce cellular water permeability. Hum Mol Genet. 17:2379-89.

Sridharan S, Brehm R, Bergmann M, Cooke PS. 2007. Role of connexin 43 in Sertoli cells of testis. Ann N Y Acad Sci. 1120:131-43.

St. Hillaire C, Vargas D, Pardo CA, Gincel D, Mann J, Rothstein JD, McArthur JC, Conant K. 2005. Aquaporin 4 is increased in association with human immunodeficiency virus dementia: implications for disease pathogenesis. J. Neurovirol. 11:535 543.

Su G, Kintner DB, Sun D. 2002. Contribution of Na(+)-K(+)-Cl(-) cotransporter to high-[K(+)](o)- induced swelling and EAA release in astrocytes. Am J Physiol Cell Physiol 282:C1136-46.

Szakacs R, Weiczner R, Mihaly A, Krisztin-Peva B, Zador Z, Zador E. 2003. Non-competitive NMDA receptor antagonists moderate seizure-induced c-fos expression

in the rat cerebral cortex. Brain Res Bull 59: 485-493.

Terry RD, DeTeresa R, Hansen LA. 1987. Neocortical cell counts in normal human adult aging. Ann Neurol. 21:530-9.

Thorne RG, Nicholson C. 2006. In vivo diffusion analysis with quantum dots and dextrans predicts the width of brain extracellular space. Proc Natl Acad Sci U S A. 103:5567-72.

Toyofuku T, Akamatsu Y, Zhang H, Kuzuya T, Tada M, Hori M. 2001. c-Src regulates the interaction between connexin-43 and ZO-1 in cardiac myocytes. J Biol Chem 276:1780-1788.

Trachtman H. 1992. Cell volume regulation: a review of cerebral adaptive mechanisms and implications for clinical treatment of osmolal disturbances: II. Pediatr Nephrol. 6:104-12.

Van Harreveld A, Malhotra SK. 1967 Extracellular space in the cerebral cortex of the mouse. J Anat. 101:197-207.

Van Harreveld A, Khattab FI. 1967 Changes in cortical extracellular space during spreading depression investigated with the electron microscope. J Neurophysiol. 30:911-29.

van Hoek AN, Verkman AS. 1992. Functional reconstitution of the isolated erythrocyte water channel CHIP28. J. Biol. Chem. 267:18267–18269.

Vaz R, Sarmento A, Borges N, Cruz C, Azevedo I. 1997. Ultrastructural study of brain microvessels in patients with traumatic cerebral contusions. Acta Neurochir (Wien). 139:215-20.

Verkman AS. 2005. More than just water channels: unexpected cellular roles of aquaporins. J Cell Sci. 118:3225-32.

Verkman AS, Binder DK, Bloch O, Auguste, K, Papadopoulos, M. C. 2006. Three distinct roles of aquaporin-4 in brain function revealed by knockout mice. Biochim. Biophys. Acta 1758:1085–1093.

Verkman, AS 2002. Physiological importance of aquaporin water channels. Ann. Med. 34:192–200.

Verkman AS 2000. Water permeability measurement in living cells and complex tissues. J. Membr. Biol. 173:73-87.

Verkman AS, Weyer P, Brown D, Ausiello DA. 1989. Functional water channels are present in clathrin-coated vesicles from bovine kidney but not from brain. J. Biol. Chem., 264:20608-20613.

Wakayama Y, Jimi T, Inoue M, Kojima H, Murahashi M, Kumagai,T, Yamashita S. 2002. Reduced aquaporin 4 expression in the muscle plasma membrane of patients

with Duchenne muscular dystrophy. Arch. Neurol. 59:431 437.

Wallraff A, Kohling R, Heinemann U, Theis M, Willecke K, Steinhauser C. 2006. The impact of astrocytic gap junctional coupling on potassium buffering in the hippocampus. J Neurosci 26:5438-5447.

Walz W, Klimaszewski A, Paterson IA. 1993. Glial swelling in ischemia: a hypothesis. Dev Neurosci 15:216-225.

Wang Y, Mehta PP, Rose B. 1995. Inhibition of glycosylation induces formation of open connexin-43 cell-to-cell channels and phosphorylation and triton X-100 insolubility of connexin-43. J Biol Chem 270: 26581-26585.

Wasterlain CG, Torack RM. 1968. Cerebral edema in water intoxication. II. An ultrastructural study. Arch Neurol. 19:79-87.

Willecke K, Eiberger J, Degen J, et al. 2002. Structural and functional diversity of connexin genes in the mouse and human genome. J Biol Chem 383:725-737.

Yamaguchi M, Wu S, Ehara K, Nagashima T, Tamaki N. 1994. Cerebral blood flow of rats with water-intoxicated brain edema. Acta Neurochir Suppl (Wien). 60:190-2.

Yang B, Verkman AS. 1997. Water and glycerol permeabilities of aquaporins 1-5 and MIP determined quantitatively by expression of epitope-tagged constructs in Xenopus oocytes. J Biol Chem. 272:16140-6.

Yang B, Verkman AS. 1997. Water and glycerol permeabilities of aquaporins 1-5 and MIP determined quantitatively by expression of epitope-tagged constructs in Xenopus oocytes. J. Biol. Chem. 272:16140-16146.

Zador E, Mendler L, ver Heyen M, Dux L, Wuytack F. 1996. Changes in mRNA levels of the sarcoplasmic/endoplasmicreticulum Ca(2+)-ATPase isoforms in the rat soleus muscle regenerating from notexin-induced necrosis. Biochem J 320:107-113.

Zador Z, Bloch O, Yao X, Manley GT. 2007. Aquaporins: role in cerebral edema and brain water balance. Prog Brain Res. 161:185-94.

Zelenina M, Zelenin S, Bondar AA, Brismar H, Aperia A. 2002. Water permeability of aquaporin-4 is decreased by protein kinase C and dopamine. Am J Physiol Renal Physiol. 283:F309-18.

Zoremba N, Homola A, Slais K, Vorísek I, Rossaint R, Lehmenkühler A, Syková E. 2008. Extracellular diffusion parameters in the rat somatosensory cortex during recovery from transient global ischemia/hypoxia. J Cereb Blood Flow Metab. 28:1665-73.